

The cosmic evolution of dust-corrected metallicity in the neutral gas[★]

Annalisa De Cia¹, Cédric Ledoux², Patrick Petitjean³, and Sandra Savaglio⁴

¹ European Southern Observatory, Karl-Schwarzschild Str. 2, 85748 Garching bei München, Germany; e-mail: adecia@eso.org

² European Southern Observatory, Alonso de Córdova 3107, Casilla 19001, Vitacura, Santiago 19, Chile

³ IAP, CNRS and Université Paris 6, 98bis Boulevard Arago, 75014 Paris, France

⁴ Physics Dept., University of Calabria, via P. Bucci, 87036, Arcavacata di Rende, Italy

Received September 19, 2017; accepted Month dd, 2017

ABSTRACT

Interpreting abundances of Damped Ly- α Absorbers (DLAs) from absorption-line spectroscopy has typically been a challenge because of the presence of dust. Nevertheless, because DLAs trace distant gas-rich galaxies regardless of their luminosity, they provide an attractive way of measuring the evolution of the metallicity of the neutral gas with cosmic time. This has been done extensively so far, but typically not taking proper dust corrections into account. The aims of this paper are to: *i*) provide a simplified way of calculating dust corrections, based on a single observed $[X/Fe]$, *ii*) assess the importance of dust corrections for DLA metallicities and their evolution, and *iii*) investigate the cosmic evolution of iron for a large DLA sample. We derive dust corrections based on the observed $[Zn/Fe]$, $[Si/Fe]$, or $[S/Fe]$, and confirm their robustness. We present dust-corrected metallicities in a scale of $[Fe/H]_{\text{tot}}$ for 266 DLAs over a broad range of z , and assess the extent of dust corrections for different metals at different metallicities. Dust corrections in DLAs are important even for Zn (typically of 0.1–0.2, and up to 0.45 dex), which is often neglected. Finally, we study the evolution of the dust-corrected metallicity with z . The DLA metallicities decrease with redshift, by a factor of 50–100 from today to ~ 12.6 billions ago ($z = 5$). When including dust corrections, the metallicity evolution is more steep than previously thought. At low z , the average DLA metallicities are ~ 0.3 dex higher than without corrections. The upper envelope of the relation between metallicity and z reaches solar metallicity at $z \lesssim 0.5$, although some systems can have solar metallicity already out to $z \sim 3$.

Key words. (galaxies:) quasars: absorption lines – galaxies: abundances – (ISM:) dust, extinction

1. Introduction

In the past 50 years, the launch of satellites with spectroscopic UV capability has opened the possibility to characterize the metal abundances in the Galactic neutral Interstellar Medium (ISM, i.e. dominated by H I and singly ionized metals, e.g. Draine 2011). A large number of studies (e.g. Jenkins 1973; Field 1974; Morton 1975; Cardelli et al. 1993; Hobbs et al. 1993; Phillips et al. 1982, 1984; Jenkins et al. 1986; Savage & Sembach 1991; Savage et al. 1992; Welty et al. 1995; Savage & Sembach 1996) has taken the opportunity to quantify the metal abundances of elements X in the Galactic ISM, $[X/H] \equiv \log(N(X)/N(H)) - \log(N(X)_{\odot}/N(H)_{\odot})$. The observed abundances show large variations, which depend on the refractory properties of the observed metals. The higher the condensation temperature of a metal (as measured in the lab), the lower its abundance that we can measure in the gas-phase (e.g. Field 1974; Jenkins et al. 1986; Cardelli et al. 1993; Hobbs et al. 1993; Phillips et al. 1982, 1984; Welty et al. 1995; Savage & Sembach 1996). It became soon evident that large fractions of the refractory metals were missing from the observed gas-phase, because they were instead locked into dust grains. This phenomenon is called dust depletion. A jump forward in the understanding of dust depletion was done by Jenkins

(2009), who discovered that the metal abundances in the ISM in the Galaxy correlate with each other. He found compelling dust depletion sequences for several metals, smoothly evolving from less to more dusty clouds in the Galactic ISM. However, until recently the study of dust depletion in the Galaxy was done by assuming that the underlying, intrinsic metallicity of the ISM is solar. Any deviation from solar abundances had been attributed to dust depletion.

De Cia et al. (2016) studied the abundances of the Galactic ISM, using data from Jenkins (2009), and Damped Lyman- α Absorbers (DLAs) at $2 \leq z \leq 4$ from the sample selected by Ledoux et al. (2006), and without making any assumption on the intrinsic metallicity. DLAs are typically subsolar-metallicity systems characterized in absorption towards distant Quasars. They are associated with gas in and around low-mass galaxies (e.g. Christensen et al. 2014), and are the largest reservoirs of neutral hydrogen in the Universe (e.g. Wolfe et al. 1995). The large neutral hydrogen columns of DLAs (defined as $N(\text{H I}) \geq 20.3$, e.g. Wolfe et al. 2005) shield the gas against ionization (which is otherwise crucial for systems with lower $N(\text{H I})$, e.g. Viegas 1995; Vladilo et al. 2001; Péroux et al. 2007; Ledoux et al. 2009; Milutinovic et al. 2010; De Cia et al. 2011, 2012; Vreeswijk et al. 2013). Thus, the metallicity measurements do not depend on difficult ionization corrections. In addition, the existence of the same correlations of relative abundances (dust depletion sequences) in different environments such as the Milky Way, the Magellanic Clouds, and DLAs suggests that DLAs behave like ISM gas, where dust grains can grow

[★] Based on observations carried out at the European Organisation for Astronomical Research in the Southern Hemisphere under ESO programmes 065.P-0038, 065.O-0063, 066.A-0624, 067.A-0078, and 068.A-0600.

in a similar way (De Cia et al. in prep.). DLA gas can in fact include different ISM-like phases such as the warm neutral medium, the cold neutral medium, and the diffuse molecular gas (e.g. Draine 2011), it can extend well outside the stellar disks as extra-planar gas, but does not have the full extent of the halo (e.g. Pontzen et al. 2008; Marasco & Fraternali 2011; Lehner et al. 2015; Tumlinson et al. 2017). Local gas-rich dwarf galaxies, which may resemble part of the DLA population at different z , are gas dominated (gas-to-baryonic fractions of 50–90%) and their main H I disks are more extended than their stellar disks by a factor of 4 on average (Lelli et al. 2016).

Because DLAs trace gas-rich galaxies out to high redshift, and regardless of their luminosity, they provide an attractive way of measuring the evolution of the metallicity of the neutral gas with cosmic time. This has been studied extensively (e.g. Prochaska et al. 2003; Kulkarni et al. 2007; Dessauges-Zavadsky 2008; Rafelski et al. 2012), but without taking the effect of dust into account. Several studies have recognized that dust depletion is an important phenomenon for DLAs too (e.g. Pettini et al. 1994; Kulkarni et al. 1997; Vladilo 1998; Pettini et al. 2000; Savaglio 2001; Ledoux et al. 2002; Prochaska & Wolfe 2002; Vladilo 2002; Dessauges-Zavadsky et al. 2006; Rodríguez et al. 2006; Meiring et al. 2006; Vladilo et al. 2011; Som et al. 2013; De Cia et al. 2013; Quiret et al. 2016; Wiseman et al. 2017). Calura et al. (2003) and Lanfranchi & Friaça (2003) have studied the chemical evolution in DLAs taking some correction for dust depletion into account, based on the dust-correction models of Vladilo (2002). Savaglio (2006) presented simplified rough dust corrections, sometimes even based on the column density of an individual metal, such as iron. We developed a method to characterize dust depletion without any assumption on the gas metallicity. This was achieved through the study of relative abundances, $[X/Y] = \log(N(X)/N(Y)) - \log(N(X)_\odot/N(Y)_\odot)$, of several metals with different nucleosynthetic and refractory properties. The amount of dust in a system can be traced by the observed $[Zn/Fe]$, because Fe is much more depleted than Zn, and the two elements tend to follow each other nucleosynthetically, at least in the metallicity range of interest here ($-2 \leq [M/H] \leq 0$, see Sect. 6). Other ratios, such as $[Ti/Si]$ or $[Si/S]$ can be also used (see correlations of these with $[Zn/Fe]$, De Cia et al. 2016), but are typically less constrained. In De Cia et al. (2016) we discovered tight correlations between relative abundances, for DLAs as well as for the Galaxy ISM. This way we could determine the dust depletion in each system, based on the observed relative abundances, and in particular $[Zn/Fe]$, and without assumptions on the reference metallicity of the gas. With this method, it is now possible to first determine the dust depletion from the relative abundances, and then correct for dust depletion and derive the dust-corrected, total gas metallicity, in a fairly accurate way.

In this paper we develop and provide a way of calculating dust-corrected metallicities (Sect. 2), which is simplified with respect to De Cia et al. (2016) and is based on an observed $[X/Fe]$. We then apply this method to the largest possible DLA sample with $[X/Fe]$ measurements and a broad range in redshift z (Sect. 3). In Sect. 4 we assess the importance of dust corrections in the DLA population. Finally, we show the evolution of the neutral gas metallicity with cosmic time (Sect. 5), taking dust corrections into account. These corrections, as we discuss below, are crucial for metal-rich systems. We discuss potential selection effects and caveats in Sect. 6, and summarize our results and conclusions in Sect. 7.

2. Dust corrections

In De Cia et al. (2016) we found robust dust-corrected metallicities based on the simultaneous study of the abundances of several metals and on the dust depletion sequences, which were globally discovered for the whole sample of DLAs and Galactic clouds. Such dust corrections, based on the observations of several metals, are the most reliable.

However, often only a limited subset of metals can be constrained. Therefore we derive and test here a simplified method to calculate dust corrections, based on a single abundance relative to Fe, $[X/Fe]$. We call this method the single-reference method.

2.1. Based on $[Zn/Fe]$

When available, this method uses $[Zn/Fe]$ to estimate the dust depletion given the depletion sequences of De Cia et al. (2016). The first step is to calculate the depletion of an element X as follows:

$$\delta_X = A_{2X} + B_{2X} \times [Zn/Fe], \quad (1)$$

where the coefficients for Fe are $A_{2Fe} = -0.01 \pm 0.03$ and $B_{2Fe} = -1.26 \pm 0.04$, and the full list of coefficients for each metal is reported in Table 3 of De Cia et al. (2016). The dust-corrected metallicity reference is then:

$$[Fe/H]_{\text{tot}} = [Fe/H] - \delta_{Fe}, \quad (2)$$

where $[Fe/H]$ are the observed abundances, and δ_{Fe} is calculated with Eq. 1. Here we choose $[Fe/H]_{\text{tot}}$ as a reference for metallicity for two reasons. First, Fe is not affected by α -element enhancement $[\alpha/Fe]$, and therefore no nucleosynthetic corrections are needed in Eq. 2. Second, Fe is among the metals that are most easily measured, and therefore most widely available. In addition, $[Fe/H]_{\text{tot}}$ is widely used as a reference for stellar abundances, which can be an useful comparison. We assign the uncertainty on $[Fe/H]_{\text{tot}}$ to be equal to the uncertainty on $[Fe/H]$, i.e. assuming no error on the dust correction. Thus, the reported uncertainties on $[Fe/H]_{\text{tot}}$ may in fact be larger.

2.2. Based on $[Si/Fe]$ or $[S/Fe]$

When $[Zn/Fe]$ is not directly observed, then the relative abundance $[Si/Fe]$ or $[S/Fe]$ can be used instead. The depletion sequences are defined as a function of $[Zn/Fe]$ (Eq. 1). However, the relative abundances $[X/Zn]$ correlate empirically with $[Zn/Fe]$ (Eq. 1 and Fig. 3 of De Cia et al. 2016), and therefore we can derive the expected $[Zn/Fe]_{\text{exp}}$ from the observed $[X/Fe]$ as follows:

$$\begin{aligned} [X/Fe] &= [X/Zn] + [Zn/Fe]_{\text{exp}} \\ &= A_{1X} + B_{1X} \times [Zn/Fe] + [Zn/Fe]_{\text{exp}} \end{aligned} \quad (3)$$

$$[Zn/Fe]_{\text{exp}} = ([X/Fe] - A_{1X}) / (B_{1X} + 1), \quad (4)$$

where $[X/Fe]$ are the observed abundances. The coefficients for Si (S) are $A_{1Si} = 0.26 \pm 0.03$ and $B_{1Si} = -0.51 \pm 0.06$ ($A_{1S} = 0.25 \pm 0.03$ and $B_{1S} = -0.23 \pm 0.07$). The full list of coefficients for each metal is reported in Table 2 of De Cia et al. (2016). The empirical correlations between $[X/Zn]$ and $[Zn/Fe]$ are observed for several metals, including α -elements. This means that possible enhancement of Si and S will be already naturally accounted for in these empirical correlations, and thus it is not necessary to make any assumption on α -element enhancement.

2.3. Robustness of the method

We test the reliability of the single-reference method on the DLA sample of De Cia et al. (2016), for which we have robust dust-corrected metallicity $[M/H]_{\text{tot}}$ based on the observations of several metals. In Fig. 1 we show a comparison between the robust dust-corrected metallicities $[M/H]_{\text{tot}} = 0$ and the dust-corrected metallicities derived with the single-reference method based on the observed $[Zn/Fe]$ (squares), $[Si/Fe]$ (triangles), and $[S/Fe]$ (diamonds). The dust-corrected metallicities calculated using the observed $[Zn/Fe]$ are the most reliable, among the single-reference metallicities, and almost perfectly trace the real dust-corrected metallicities. The $[Si/Fe]$ and $[S/Fe]$ single-reference metallicities overall follow the real dust-corrected metallicities. However, for $[Si/Fe]$, the single-reference metallicities are a bit underestimated at low metallicity (by -0.25 dex at $[M/H]_{\text{tot}} = -2$) and a bit overestimated at high metallicity (by 0.2 dex at $[M/H]_{\text{tot}} = 0$). This is visible from the fit to the data in Fig. 1. To account for this effect and avoid related biases, we further correct the $[Fe/H]_{\text{tot}}$ that we derive with the single reference method by the difference between the fit in Fig. 1 and the one-to-one line, which varies a bit with metallicity. While for Zn-based measurements this is negligible, this affects mostly the Si-based measurements, by an average of 0.18 dex, with a standard deviation of 0.15 dex. The main effect of this additional correction is at high- z , where Si-based measurements are dominant, and it is most notable for systems with very low intrinsic metallicity, the most extreme cases being a correction of 0.44 dex at a $[Fe/H]_{\text{tot}} = -2.95$ which was corrected to $[Fe/H]_{\text{tot}} = -2.51$ to account for the Si trend in Fig. 1.

While the $[S/Fe]$ dust corrections seem more accurate than those based on $[Si/Fe]$, we caution that S may be a troublesome element because the available data to characterize the dust depletion is still limited, and specially for the Galaxy (Jenkins 2009; De Cia et al. 2016), adding some level of uncertainty on the use of S as reference. Thus, we derive dust corrections with the single-reference method using $[Zn/Fe]$ when available, otherwise $[Si/Fe]$, or otherwise $[S/Fe]$.

We note that in Fig. 1 there are two strong outliers in the relations, all associated with Si measurements with fairly large errors, namely Q 1444-014 and Q 2359-022¹. This has no tangible effect for this work, because we aim at characterizing the whole population and such outliers are statistically not important. However, possible fluctuations should be taken into account when using the single-reference method based on $[Si/Fe]$ to correct for dust in a given individual system.

The potential non-accuracy of the column density measurements may introduce some bias, in particular for the large sample (see Sect. 3). Indeed, in 47 cases the $[Zn/Fe]_{\text{exp}}$ is negative in the large sample², resulting in a non-physical positive depletion, for which we assign $\delta_X \equiv 0$ (i.e. no dust correction needed). However, only 3 out of these systems have actual Zn measurements ($[Zn/Fe] = -0.15, -0.32, -0.02$ dex), the others are derived from either $[Si/Fe]$ or $[S/Fe]$. As a comparison, for the clean sample the $[Zn/Fe]_{\text{exp}}$ is negative only in two cases, and only by a small amount (i.e. $-0.08, -0.19$ dex). Therefore the 47 negative $[Zn/Fe]_{\text{exp}}$ in the large sample are likely the product of inaccurate estimates of the column densities, and perhaps in a small part because of small nucleosynthetic effects, as we discuss below.

¹ Q 1444-014 and Q 2359-022 are presented in Ledoux et al. (2003) and De Cia et al. (2016), respectively, and their Si II column density appears to be reasonably well estimated.

² down to -1.5 dex, with a mean and standard deviation of -0.3 and 0.4 , respectively. See Table A.2 for the individual values.

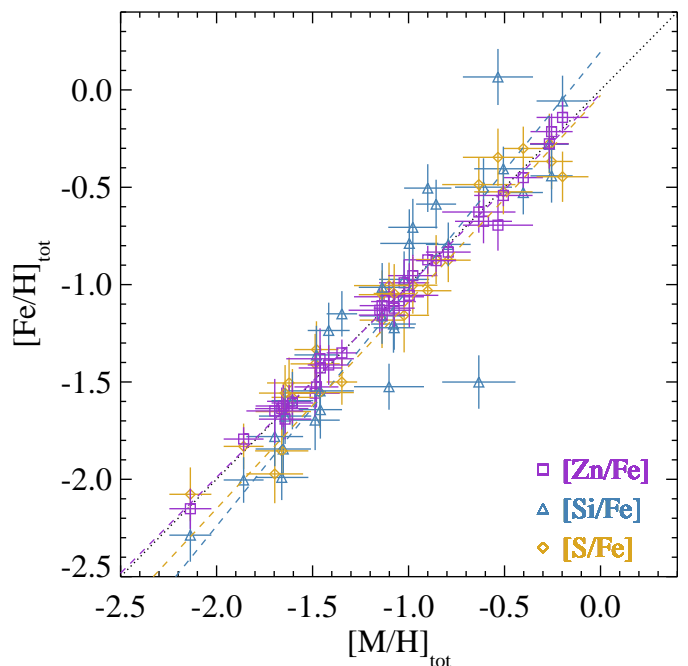


Fig. 1. Comparison between the solid dust-corrected metallicities $[M/H]_{\text{tot}}$ derived by De Cia et al. (2016) from several metals simultaneously and the dust-corrected metallicities $[Fe/H]_{\text{tot}}$ derived with the single-reference method (Sect. 2). The linear fits to the data (dashed curves) have slopes of 0.98, 1.22, and 1.06 for Zn, Si, and S, respectively, and intercepts of -0.02 , 0.19 , and -0.03 . The differences from the one-to-one line are taken into account in the paper for the final calculation of the $[Fe/H]_{\text{tot}}$.

Statistically, these random inaccuracies on the column densities would tend to cancel each other, and not bring a strong bias in our results for the large sample.

3. Data

We calculate dust-corrected metallicities $[Fe/H]_{\text{tot}}$ for DLAs taken from different samples. First, we include the DLAs from De Cia et al. (2016), which have solid dust-corrected metallicities derived from studying simultaneously all metals. Then we select the DLAs using two approaches, which we call the clean and the large samples, as explained below.

3.1. The clean sample

We select DLAs that have high-quality data and which abundances can be trusted, in the sense that are all based on high-resolution spectroscopy and we have checked them thoroughly. For this we resort to the 'quality' selection of Møller et al. (2013), which includes data from Ellison et al. (2012), Péroux et al. (2006), Pettini et al. (2000), Péroux et al. (2008), Rao et al. (2005), Meiring et al. (2011), Pettini et al. (1999) at $z < 2$, and Ledoux et al. (2006) and Rafelski et al. (2012) at higher z . We also include the more recent metal-rich DLAs from Ma et al. (2015) and Fynbo et al. (2017). The purpose of the clean sample is to monitor the corrections that we need to apply to metallicities due to dust depletion, based on reliable relative abundances. However, this selection is not necessarily representative of the whole DLA population. In particular, the paucity of DLAs at high and low redshift makes it statistically incomplete. We therefore do not use this sample

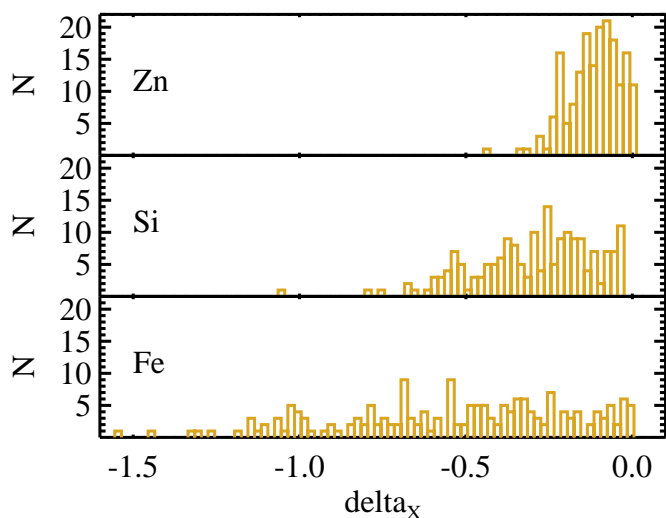


Fig. 2. Distribution of the dust corrections (i.e. depletions) for Zn, Si, and Fe that we calculate for the large sample.

to assess the evolution of metallicity with redshift, but only to control the required dust corrections. To bypass this lack of completeness, we also consider the largest available DLA sample, below. Further potential biases are discussed in Sect. 5.

3.2. The large sample

We apply the dust correction to as many DLA abundances as available in the literature, with sufficient relative abundances measurements to derive a sensible dust-correction. For this, we source the recent literature collection of Berg et al. (2015).³ We also include the more recent metal-rich DLAs from Ma et al. (2015) and Fynbo et al. (2017). The total number of DLAs in this sample is 266, which is comparable with the sample of Rafelski et al. (2012) and its high- z extension (Rafelski et al. 2014) all together. While the sample of Berg et al. (2015) is originally much larger (almost 400 DLAs), we filtered those DLAs where Fe and at least another metal were well constrained to allow proper dust corrections. The purpose of the large sample is to provide dust-corrections for all literature DLAs, and furthermore to investigate the evolution of dust-corrected metallicity with redshift. Possible biases are discussed in Sect. 6.

4. The importance of dust corrections

Dust corrections are important, and crucial for metal-rich systems. Figure 2 shows the overall distributions of depletions for Zn, Si, and Fe, in the large sample. Figure 3 shows the extent of the depletions of Zn, Si, and Fe in the clean sample with the dust-corrected metallicity. Each individual system is represented by a value of δ_{Zn} , δ_{Si} , and δ_{Fe} in this plot. Clearly, the dust corrections increase with metallicity. Typically Zn is depleted by ~ 0.1 – 0.2 dex in most DLAs, but depletes up to 0.45 dex for the most metal rich systems (e.g. J1211+0833 Ma et al. 2015). As a comparison, in the Galaxy Zn depletes up to 0.67 dex in the dustiest Galactic lines of sight (ζ Oph, e.g. Savage & Sembach 1996).

³ There is a small discrepancy between the $\log N(\text{H I})$ for J1208+0010 between the values originally reported by Rafelski et al. (2014) and later by Berg et al. (2015). We use the former value $\log N(\text{H I}) = 20.30 \pm 0.15$, because regarded as more reliable (Berg, private communication).

Therefore $[\text{Zn}/\text{H}]$ is not a dust-free measurement of metallicity, and thus not necessarily a good metallicity estimator without dust corrections. Silicon and iron deplete up to 1.06 and 2.10 dex, respectively, in our samples. Even for less dusty, metal-poor end, Zn, Si, and even more Fe, can be still easily depleted, of about ~ 0.1 , ~ 0.3 , and ~ 0.5 dex for systems with $[\text{Zn}/\text{Fe}] = 0.4$, for Zn, Si, and Fe, respectively. While a significant fraction of DLAs have very little dust depletion, and therefore has a low dust and metal content (as well as molecules, e.g. Petitjean et al. 2000; Noterdaeme et al. 2008; Ledoux et al. 2009), it is evident that systems with more dust and molecules do exist and are an important part of the DLA population.

The $[\text{Fe}/\text{H}]_{\text{tot}}$ is a measure of the total, dust-corrected metallicity, without influence of α -element enhancement. These can be compared to stellar $[\text{Fe}/\text{H}]$. However, while stellar abundances typically have a wide range of abundances for a given galaxy (e.g. Tolstoy et al. 2009), the ISM is the product of a longer-term reprocessing and recycling of metals in the gas, and has a narrower range of metallicities (e.g. Krumholz & Ting 2017). For the Galaxy, the neutral ISM metallicity is typically assumed to be solar (e.g. Savage & Sembach 1996; Jenkins 2009). In addition, there may be some ISM metallicity gradients from the inner to the outer regions of the galaxies, which for DLAs should be shallow (e.g. 0.022 dex/kpc Christensen et al. 2014). The position of the knee of the α -element enhancement distribution depends on the mass of the galaxy, where lower mass galaxies show the α -element knee at lower metallicities Tolstoy et al. (2009); de Boer et al. (2014). When dust depletion is taken into account, the intrinsic $[\alpha/\text{Fe}]$ in DLAs are not strongly enhanced (as also remarked by Vladilo 2002). α -element enhancement levels similar to the Galaxy have been observed in DLAs with low-metallicity (De Cia et al. 2016). Further analysis on the $[\alpha/\text{Fe}]$ in DLAs will be presented in De Cia et. al., in preparation.

5. Metallicity evolution with cosmic time

Figure 4 shows the evolution of dust-corrected $[\text{Fe}/\text{H}]_{\text{tot}}$ with z for the 266 DLAs of the large sample. The dust-corrected metallicities for the clean and the large sample are reported in Table A.1 and A.2, respectively. The black filled circles are the solid metallicity measurements from De Cia et al. (2016), which were derived from several metal relative abundances simultaneously. The colored open symbols are the $[\text{Fe}/\text{H}]_{\text{tot}}$ that we derived as described in Sect. 2, and where the dust corrections were calculated based on $[\text{Zn}/\text{Fe}]$, or $[\text{Si}/\text{Fe}]$, or $[\text{S}/\text{Fe}]$, as labeled. The solid line shows a linear fit to the data, where errors on both x and y data are considered, and including the intrinsic scatter σ_{int} .⁴ The dotted lines show the extent of the intrinsic scatter resulting from this fit. The results from the linear fit to the data are reported in Table 1.

We compare our results with those of Rafelski et al. (2012), because it was the largest study of DLA metallicity evolution with z until now. The dashed blue curve shows the mean DLA metallicity $[\text{Si}/\text{H}] = -0.65 + (-0.22 \times z)$ of Rafelski et al. (2012), which was derived without dust-corrections. The drop at high

⁴ This is a linear least-squares approximation in one dimension ($y = a + bx$) that considers errors on x and y data (σ_x and σ_y), using the IDL routine MPFITEXY (Williams et al. 2010). MPFITEXY utilizes the MPFIT package (Markwardt 2009). Each data point is weighted as $1/\sqrt{\sigma_x^2 + b^2\sigma_y^2 + \sigma_{\text{int}}^2}$, where σ_{int} is the intrinsic scatter of the data around the model (“Nukers’ Estimate”; Tremaine et al. 2002). The value σ_{int} is automatically scaled to produce a reduced $\chi^2_{\nu} \sim 1$. We adopt an initial guess for σ_{int} of 0.1 dex.

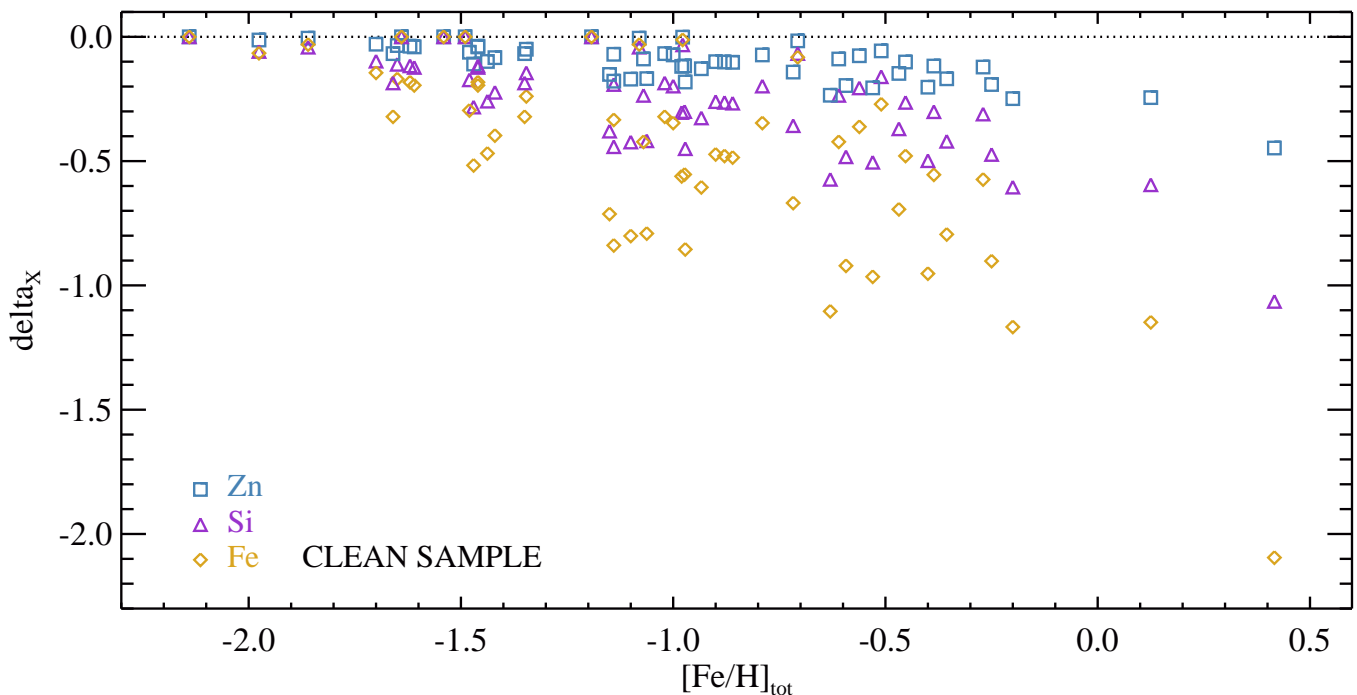


Fig. 3. The depletions of Zn, Si, and Fe in the clean sample (Sect. 3), with the dust-corrected metallicity $[\text{Fe}/\text{H}]_{\text{tot}}$. Each individual system is represented by a value of δ_{Zn} , δ_{Si} , and δ_{Fe} .

redshift is an extrapolation of the results of Rafelski et al. (2014), which extended the analysis of Rafelski et al. (2012) with a sample of high- z DLAs. We stress that in Fig. 4 we show a scale of $[\text{Fe}/\text{H}]_{\text{tot}}$, while Rafelski et al. (2012) and Rafelski et al. (2014) used a scale of $[\text{Si}/\text{H}]$. These authors use either the observed Zn, Si or S metallicity, or otherwise the Fe metallicity enhanced by a systematic value of 0.3 dex to compensate for possible α -element enhancement.⁵ Thus, the dashed blue curve may in fact be lower than in Fig. 4. Nevertheless, we decide not to apply any shift, because the α -element enhancement is likely metallicity dependent, and we do not make any assumption on $[\alpha/\text{Fe}]$ in this work.

We also compare our results with those of Vladilo (2002), who studied the cosmic evolution of iron metallicity in a small sample of DLAs including independent dust corrections. We obtain the exact same slope of the metallicity evolution found by Vladilo (2002), which is a reassuring result for both methods. The improvement with respect of the former work is more simplicity and less assumptions for the dust-correction method presented here, and the larger size of the DLA sample.

The metallicity of DLAs decreases with z , and the correlation is significant, as confirmed by the correlation coefficients and low null-hypothesis probabilities (reported in Table 1). The slope that we find is 0.1 dex per unit z steeper than what was previously found by Rafelski et al. (2012), where no dust corrections were applied. Interestingly, the evolution of metallicity with z that can be found using DLAs (in absorption) is much steeper than what has been found for galaxies in emission, even taking different mass bins into account, while the low- z results may be consistent (e.g. Hunt et al. 2016). Determining the metallicity from emission lines may be challenging at high z (e.g.

Kewley & Ellison 2008). However, we expect the gas probed by DLAs to be physically more extended than the classical ISM that is illuminated by stars in disks and shows the strong emission lines. Thus, the metallicities in absorption and emission do not have to necessarily agree. Comparing our results for the neutral gas with the metallicity evolution of the ionized gas, traced by lower H I absorbers ($\log N(\text{H I}) < 19$), we confirm that DLAs lack the very low metallicities observed in low H I systems, which are thought to be related to the circumgalactic or intergalactic medium (Lehner et al. 2016).

In the analysis of our samples we find a significant difference with the previous results on the metallicity evolution of the neutral gas at low z , i.e. about 0.3 dex higher metallicities than without taking dust corrections into considerations (Rafelski et al. 2012). This arises mostly from the fact that it is indeed in the metal-rich regime that dust depletion is the strongest, and even for Zn and Si, which is often not considered. On the high- z end, more DLA measurements are needed to solidly compare to previous results (e.g. Rafelski et al. 2014).

The relation of metallicity with cosmic time shows a large scatter, of about 0.5 dex, similarly to what had been previously found by, for example, Rafelski et al. (2012) and Neeleman et al. (2013). At any given z , we expect that DLAs may select galaxies with a range of different masses and metallicities. Thus, the scatter of the metallicity vs cosmic time relation is physical, and it reflects a spread in metallicity (and mass, due to the mass-metallicity relation, e.g. Tremonti et al. 2004). Galaxies with lower masses and metallicities are expected to lie in the lower envelope of the relation of metallicity with cosmic time, and galaxies with higher masses and metallicities in the upper envelope. Massive galaxies like the Milky Way are rare among DLAs, but they do exist (e.g. Ma et al. 2015). Interestingly, the upper envelope of the metallicity vs cosmic time relation at low z reaches solar metallicities, and a few DLAs have supersolar metallicity at moderate z . For a discussion on the mass-metallicity relation in DLAs and its extensions

⁵ This also artificially compensates for some dust depletion by a mean depletion of iron of 0.3 dex into dust. However, this value is arbitrary and is far from the necessary dust corrections for Fe in DLAs, as we discuss below.

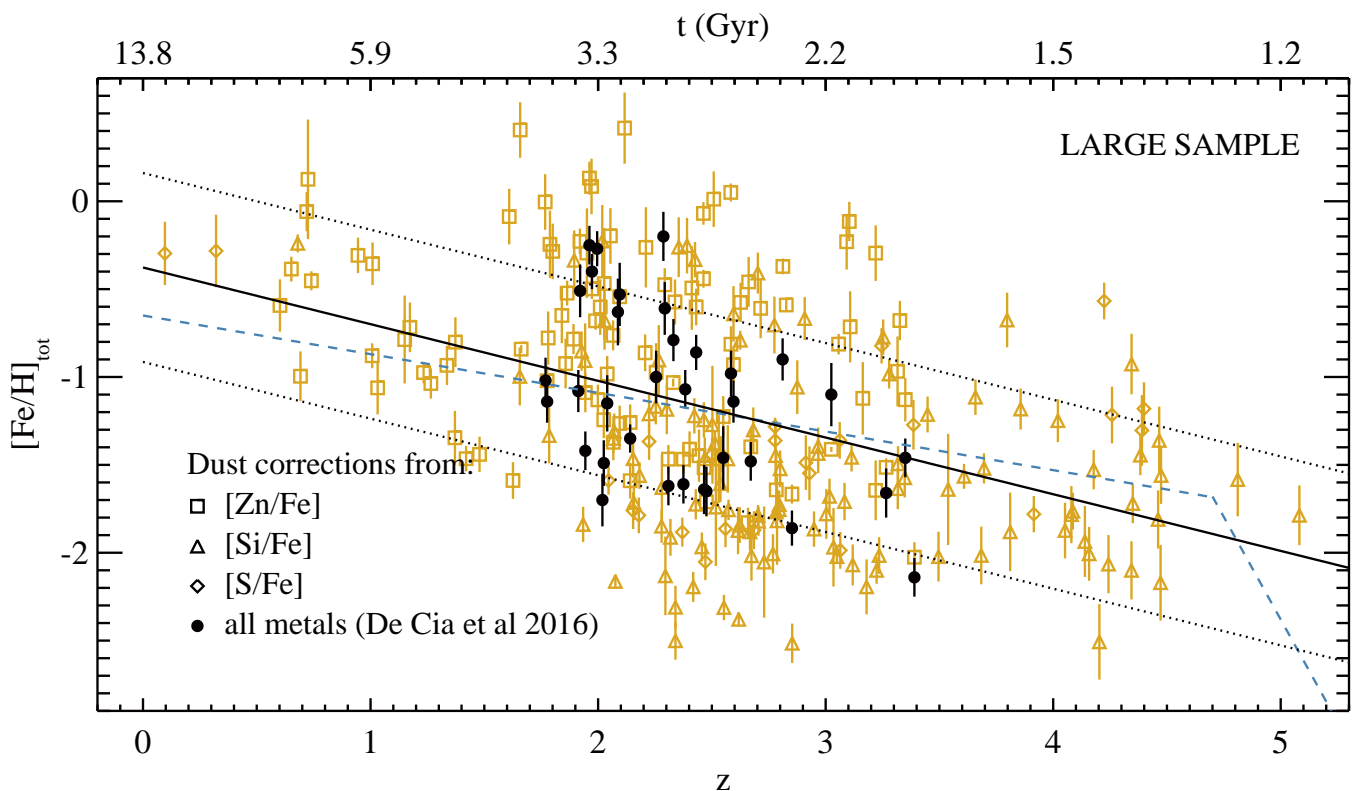


Fig. 4. The dust-corrected metallicities $[M/H]_{\text{tot}}$ derived from several metals simultaneously by De Cia et al. (2016, black filled circles), and the dust-corrected metallicities $[\text{Fe}/\text{H}]_{\text{tot}}$ calculated with the single-reference method (Sect. 2) for the large sample (gold open symbols). The shape of the symbols show which reference was used for the dust correction, as labeled. The black solid and dotted lines display the linear fit to the data and the intrinsic scatter of the relation, respectively. The dashed blue curve shows the average DLA metallicity derived by Rafelski et al. (2012) - originally derived for a scale of $[\text{Si}/\text{H}]$ - and the drop at high z found by Rafelski et al. (2014).

see Ledoux et al. (2006), Prochaska et al. (2008), Møller et al. (2013), Neeleman et al. (2013), Christensen et al. (2014), and Arabsalmani et al. (2015). The extent of the scatter can in principle carry important information on these scaling relations. However, selection biases and incompleteness influence the extent of this scatter. For example, the fact that the scatter seems larger at $2 \lesssim z \lesssim 3.5$ is the effect of lower and higher z ranges having less measurements due to an observational bias, as we discuss in the next Section.

In Fig. 4 we show a linear fit to the metallicities with respect to redshift, and show the cosmic time scale, converted using the relation between time and redshift for a flat Universe (e.g. Thomas & Kantowski 2000), and assuming $H_0 = 67.8$ and $\Omega_M = 0.308$ (Planck Collaboration et al. 2016). A linear fit to the data along the time axis does not provide a good description of the data, specially at low and high z , meaning that the distribution of metallicity with time is not linear. This is in accordance with cosmic chemical evolution models, which generally predict an evolution of metallicity with cosmic time that is linear with z , at least out to $z \sim 4$ or so (e.g. Pei & Fall 1995; Calura et al. 2003; Tumlinson 2010; Matteucci 2012; Gioannini et al. 2017). In the linear time frame, this reflects a flattening of the increase of metallicity below $z \sim 1-2$. Indeed, the cosmic starformation density (and, broadly speaking, the buildup of metals) increases with the age of the Universe and peaks around $z \sim 1-2$ (e.g. Madau et al. 1998). While we find overall agreement between our observations and some chemical evolution models (e.g. Pei & Fall 1995; Tumlinson 2010), a careful comparison with different models is beyond the scope of this paper and should be addressed in detail in the future.

6. Biases, (in)completeness, and caveats

Through DLAs we probe the evolution of the metallicity of the neutral gas with cosmic time. The mean metallicities that we find are not necessarily representative of the mean metallicity of galaxies or the mean metallicity of the Universe, and they only refer to the neutral gas content of galaxies. In this section we discuss what are the possible biases that could affect our selection of DLAs with respect to the global population of DLAs.

Typical flux-limited studies of galaxies (i.e. observing the stellar, gas, molecular, or dust emission) are biased towards the brightest objects. This is not true for DLAs, although potential dust obscuration may have an effect on the selection of the background QSOs themselves, as we discuss below. DLA-selected galaxies do not suffer from this bias against faintest targets, but instead from different and complementary biases. DLAs are selected from the cross-section of the gas around galaxies of different kinds, including low-mass faint galaxies. While the gas in larger galaxies can extend to larger distances (see Fynbo et al. 2008; Krogager et al. 2017, for how this impacts DLA selection and searches), low-mass galaxies are the most common in number (e.g. Fontana et al. 2004).

As mentioned above, the selection of QSOs behind DLAs may be biased by the presence of dust in the absorbers. Indeed, if the background QSO is obscured by dust, it may simply be missed by the surveys. Some studies have suggested that this could be a strong bias (e.g. Vladilo & Péroux 2005). On the other hand, low reddening has been found in most systems, also when including dust-independent selection methods of the QSO (e.g. radio or X-ray selections, Ellison et al. 2005; Vladilo et al. 2008;

Table 1. Coefficients of the linear fit ($[\text{Fe}/\text{H}]_{\text{tot}} = A + B \times z$) to the data in Fig. 4. σ_{int} is the intrinsic scatter of the correlations. r and ρ are the Pearson and Spearman correlation coefficients, respectively, and are listed with their respective null-probability (p_r and p_ρ).

Sample	A	B	σ_{int}	r	p_r	ρ	p_ρ
LARGE	-0.38 ± 0.11	-0.32 ± 0.04	0.54	-0.45	$2.E - 14$	-0.47	$7.E - 16$

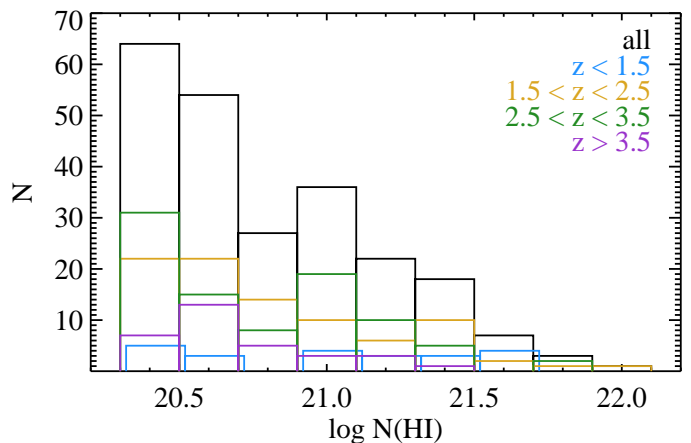
Krogager et al. 2016a). Moderately highly reddened systems are rare but exist (Krogager et al. 2016b; Fynbo et al. 2017). The effect of dust obscuration acts more strongly on systems with higher dust columns, perhaps more dusty and metal-rich systems which are more common at low z . If we were missing some of these metal-rich and dusty systems at low- z , the metallicity evolution curve could be even steeper than what we find. However, at high z the rest-frame UV emission of the background QSOs is more efficiently absorbed by dust than the low- z rest-frame optical (e.g. Savaglio 2015). Thus, this bias may be stronger at high z , but on the other hand there is decreasing dust content at higher z , mitigating this effect. Overall, the dust obscuration bias should be small given what we have discussed above, but quantifying this effect is beyond the scope of this paper. Pontzen & Pettini (2009) have quantified that only 7% of DLAs may be missing due to dust obscuration bias.

Another bias that may be dependent on z is the metal selection. Because Zn is more difficult to measure due to its fairly weak lines, it is virtually never observed at high z (never at $z > 3.5$ in our large sample). On the high- z end, the easiest and common metals to measure are Si and Fe. As we discussed in Sect. 2, there is some effect on the dust corrections calculated only based on the observed $[\text{Si}/\text{Fe}]$, and these affect mainly the very low metallicity systems by underestimating their metallicity (making a slightly steeper metallicity evolution curve). In this paper we have corrected for this effect, but it is useful to keep this in mind.

In addition, low- z DLAs are selected in a different way than at high z . Indeed, $\text{Ly-}\alpha$ is redshifted into the optical range above $z \gtrsim 2$, and the DLA identification can be done from ground-based observations. On the other hand, UV observations are needed to identify low- z DLAs, and these are often selected from Mg II absorbers (e.g. Petitjean & Bergeron 1990; Rao & Turnshek 2000), which may in principle have different overall properties than classical DLAs, such as higher metallicity. However, this effect seems negligible, i.e. the Mg II-selected DLAs do not show higher metallicities than the non-Mg II-selected DLAs (Rao et al. 2017).

On the high- z end, estimating H I is increasingly challenging because of the $\text{Ly-}\alpha$ forest becoming more crowded. The H I column density measurements must rely on the onset of the red dumping wing, and this may perhaps introduce large systematic uncertainties (> 0.3 dex).

The completeness of the sample determines how well the given set of data represents the overall population of DLAs, and this also varies with z . Indeed, the majority of DLAs are observed at $2 \lesssim z \lesssim 3.5$. One way of assessing the completeness of our sample is by studying its $N(\text{H I})$ distribution, which is shown in Fig. 5 for different redshift intervals. In the redshift range of about $1.5 < z < 3.5$ the $N(\text{H I})$ distribution is similar to that of the large Sloan Digital Sky Survey (SDSS-DR5) DLA sample (Prochaska et al. 2005), and of the Ultraviolet and Visual Echelle Spectrograph (UVES) DLA sample of Noterdaeme et al. (2008), which was scaled to compensate for completeness biases. In this z interval we can therefore assume that the completeness is high, also given that other biases discussed above seem to be limited.

**Fig. 5.** The distribution of $\log N(\text{H I})$ for the large sample (all), and sub-samples at particular redshift interval, as labeled.

On the other hand, at lower and higher z the sample is still relatively small, and therefore we are missing the most extreme and rarest objects, on both the high- and low-metallicity envelopes of the metallicity evolution curve. For example high- $N(\text{H I})$ systems are missing in at low and high z (see Fig. 5), although these systems are very rare (Noterdaeme et al. 2014). Incompleteness is particularly severe at $z \lesssim 0.5$ and $\gtrsim 4.5$, where only a few measurements are available in our sample. The scatter of the metallicity evolution with redshift is heavily affected by incompleteness at high and low z , and we therefore refrain from studying it further in this paper.

In this paper we derive dust corrections based on the observed or expected $[\text{Zn}/\text{Fe}]$. The underlying assumption is that Zn and Fe trace each other nucleosynthetically. A flat $[\text{Zn}/\text{Fe}]$ (and slightly supersolar) is indeed observed in the Galaxy ISM, for $-2 \leq [M/\text{H}] \leq 0$ (e.g. Sneden et al. 1991). There are strong (+0.5 dex) deviations from this at lower ($[M/\text{H}] < -3$) and higher metallicities (e.g. Primas et al. 2000; Nissen et al. 2007). In addition, the mere existence of narrow dust depletion sequences for the Galaxy as well as DLAs (De Cia et al. 2016) limits the possible scatter in the nucleosynthetic $[\text{Zn}/\text{Fe}]$ of the current sample to be < 0.2 dex. While small deviations from a solar $[\text{Zn}/\text{Fe}]$ are possible, as mentioned above, we exclude large nucleosynthetic effects on the $[\text{Zn}/\text{Fe}]$ abundances. Indeed, we do not measure heavily negative $[\text{Zn}/\text{Fe}]$ in DLAs. Stellar measurements of $[\text{Zn}/\text{Fe}]$ can vary dramatically, in gas-poor environments such as dwarf spheroidals (Skúladóttir et al. 2017) and the inner bulge of the Milky Way (Barbuy et al. 2015; Duffau et al. 2017). However, gas-rich environment, such as the Milky Way disk, the Magellanic Clouds, and DLAs, do not show this effect in their gas component (e.g. De Cia et al. in prep.), where the contribution from different stellar populations have slowly been reprocessed in the gas. It is possible that the $[\text{Zn}/\text{Fe}]$ zero-point is slightly off, perhaps down to -0.2 dex, as discussed in De Cia et al. (2016). The truncation in the distribution of the δ_{Zn} (Fig. 2) may also support the possibility of such small off-

set. In the $[Zn/Fe] = -0.2$ dex offset case, Si would be depleted by 0.1 dex more heavily than with the current assumption, and much less than this for S and Zn. This would slightly push up the metallicity, by less than 0.1 dex, at the high- z end.

7. Summary and conclusions

We develop a simplified method for calculating dust corrections to metal abundances (which we called the single-reference method), and confirm the robustness of this method by comparing the dust corrections to the solid ones derived by De Cia et al. (2016) by studying several metals simultaneously. We apply the new dust corrections to two DLA samples with published abundances: *i*) a selection of high-quality measurements (the clean sample), and *ii*) the largest number of available measurements (the large sample). From our analysis we conclude the following.

1. Dust corrections are important. Even Zn, which is often considered undepleted, can be depleted in DLAs, by typically 0.1–0.2 dex and up to 0.45 dex (Sect. 4).
2. Dust corrections are most crucial for more metal-rich systems. The depletions of Zn, Si, and Fe are shown in Fig. 3 as a function of dust-corrected metallicity.
3. The DLA metallicities decrease with redshift. After including dust corrections, the slope of the metallicity decline with z is steeper than what had previously found. Our best fit to the large sample yields $[Fe/H]_{\text{tot}} = -0.30 - 0.39 \times z$, with a large internal scatter of 0.6 dex (Sect. 5).
4. The average DLA metallicity at low z is ~ 0.3 dex higher than what previously thought, when taking dust corrections into account.
5. We do not find evidence for a steepening of the evolution of metallicity at high z . However, more measurements are needed to draw solid conclusions on the high- z regime.
6. We derived the cosmic evolution of dust-corrected metallicity of iron in the neutral gas, $[Fe/H]_{\text{tot}}$. This scale carries no assumptions on the α -element enhancement.
7. The scatter of the relation of metallicity with z is physical. At any given z a range of galaxies metallicities (and masses) is indeed expected. However, possible biases due to selection effects may affect the extent of the scatter.
8. The upper envelope of the relation of metallicity with z reaches solar metallicity at low z .
9. We confirm that the DLA metallicity evolution with cosmic time supports the scenario where DLAs are associated with gas in and around galaxies with a wide range in metallicity and mass. While they have predominantly low metallicities and masses, DLAs can occasionally select also more metal-rich and massive systems.
10. The dust-corrected metallicity of the neutral gas in galaxies decreases by a factor of ~ 50 –100 from today to $z = 5$.

References

Arabsalmani, M., Møller, P., Fynbo, J. P. U., et al. 2015, MNRAS, 446, 990
 Barbuy, B., Friaça, A. C. S., da Silveira, C. R., et al. 2015, A&A, 580, A40
 Berg, T. A. M., Ellison, S. L., Prochaska, J. X., Venn, K. A., & Dessauges-Zavadsky, M. 2015, MNRAS, 452, 4326
 Calura, F., Matteucci, F., & Vladilo, G. 2003, MNRAS, 340, 59
 Cardelli, J. A., Federman, S. R., Lambert, D. L., & Theodosiou, C. E. 1993, ApJ, 416, L41
 Christensen, L., Møller, P., Fynbo, J. P. U., & Zafar, T. 2014, MNRAS, 445, 225
 de Boer, T. J. L., Belokurov, V., Beers, T. C., & Lee, Y. S. 2014, MNRAS, 443, 658
 De Cia, A., Jakobsson, P., Björnsson, G., et al. 2011, MNRAS, 412, 2229

De Cia, A., Ledoux, C., Fox, A. J., et al. 2012, A&A, 545, A64
 De Cia, A., Ledoux, C., Mattsson, L., et al. 2016, A&A, 596, A97
 De Cia, A., Ledoux, C., Savaglio, S., Schady, P., & Vreeswijk, P. M. 2013, A&A, 560, A88
 Dessauges-Zavadsky, M. 2008, in IAU Symposium, Vol. 255, Low-Metallicity Star Formation: From the First Stars to Dwarf Galaxies, ed. L. K. Hunt, S. C. Madden, & R. Schneider, 121–128
 Dessauges-Zavadsky, M., Prochaska, J. X., D’Odorico, S., Calura, F., & Matteucci, F. 2006, A&A, 445, 93
 Draine, B. T. 2011, Physics of the Interstellar and Intergalactic Medium (Princeton University Press)
 Duffau, S., Caffau, E., Sbordone, L., et al. 2017, ArXiv e-prints [arXiv:1704.02981]
 Ellison, S. L., Hall, P. B., & Lira, P. 2005, AJ, 130, 1345
 Ellison, S. L., Kanekar, N., Prochaska, J. X., Momjian, E., & Worseck, G. 2012, MNRAS, 424, 293
 Field, G. B. 1974, ApJ, 187, 453
 Fontana, A., Pozzetti, L., Donnarumma, I., et al. 2004, A&A, 424, 23
 Fynbo, J. P. U., Krogager, J.-K., Heintz, K. E., et al. 2017, ArXiv e-prints [arXiv:1706.07016]
 Fynbo, J. P. U., Prochaska, J. X., Sommer-Larsen, J., Dessauges-Zavadsky, M., & Møller, P. 2008, ApJ, 683, 321
 Giannini, L., Matteucci, F., & Calura, F. 2017, MNRAS, 471, 4615
 Hobbs, L. M., Welty, D. E., Morton, D. C., Spitzer, L., & York, D. G. 1993, ApJ, 411, 750
 Hunt, L., Dayal, P., Magrini, L., & Ferrara, A. 2016, MNRAS, 463, 2002
 Jenkins, E. B. 1973, ApJ, 181, 761
 Jenkins, E. B. 2009, ApJ, 700, 1299
 Jenkins, E. B., Savage, B. D., & Spitzer, Jr., L. 1986, ApJ, 301, 355
 Kewley, L. J. & Ellison, S. L. 2008, ApJ, 681, 1183
 Krogager, J.-K., Fynbo, J. P. U., Heintz, K. E., et al. 2016a, ApJ, 832, 49
 Krogager, J.-K., Fynbo, J. P. U., Noterdaeme, P., et al. 2016b, MNRAS, 455, 2698
 Krogager, J.-K., Møller, P., Fynbo, J. P. U., & Noterdaeme, P. 2017, MNRAS, 469, 2959
 Krumholz, M. R. & Ting, Y.-S. 2017, ArXiv e-prints [arXiv:1708.06853]
 Kulkarni, V. P., Fall, S. M., & Truran, J. W. 1997, ApJ, 484, L7
 Kulkarni, V. P., Khare, P., Péroux, C., et al. 2007, ApJ, 661, 88
 Lanfranchi, G. A. & Friaça, A. C. S. 2003, MNRAS, 343, 481
 Ledoux, C., Bergeron, J., & Petitjean, P. 2002, A&A, 385, 802
 Ledoux, C., Petitjean, P., & Srianand, R. 2003, MNRAS, 346, 209
 Ledoux, C., Petitjean, P., & Srianand, R. 2006, ApJ, 640, L25
 Ledoux, C., Vreeswijk, P. M., Smette, A., et al. 2009, A&A, 506, 661
 Lehner, N., Howk, J. C., & Wakker, B. P. 2015, ApJ, 804, 79
 Lehner, N., O’Meara, J. M., Howk, J. C., Prochaska, J. X., & Fumagalli, M. 2016, ApJ, 833, 283
 Lelli, F., McGaugh, S. S., & Schombert, J. M. 2016, AJ, 152, 157
 Ma, J., Caugal, P., Noterdaeme, P., et al. 2015, MNRAS, 454, 1751
 Madau, P., Pozzetti, L., & Dickinson, M. 1998, ApJ, 498, 106
 Marasco, A. & Fraternali, F. 2011, A&A, 525, A134
 Markwardt, C. B. 2009, in Astronomical Society of the Pacific Conference Series, Vol. 411, Astronomical Data Analysis Software and Systems XVIII, ed. D. A. Bohlender, D. Durand, & P. Dowler, 251
 Matteucci, F. 2012, Chemical Evolution of Galaxies
 Meiring, J. D., Kulkarni, V. P., Khare, P., et al. 2006, MNRAS, 370, 43
 Meiring, J. D., Tripp, T. M., Prochaska, J. X., et al. 2011, ApJ, 732, 35
 Milutinovic, N., Ellison, S. L., Prochaska, J. X., & Tumlinson, J. 2010, MNRAS, 408, 2071
 Møller, P., Fynbo, J. P. U., Ledoux, C., & Nilsson, K. K. 2013, MNRAS, 430, 2680
 Morton, D. C. 1975, ApJ, 197, 85
 Neelaman, M., Wolfe, A. M., Prochaska, J. X., & Rafelski, M. 2013, ApJ, 769, 54
 Nissen, P. E., Akerman, C., Asplund, M., et al. 2007, A&A, 469, 319
 Noterdaeme, P., Ledoux, C., Petitjean, P., & Srianand, R. 2008, A&A, 481, 327
 Noterdaeme, P., Petitjean, P., Pâris, I., et al. 2014, A&A, 566, A24
 Pei, Y. C. & Fall, S. M. 1995, ApJ, 454, 69
 Péroux, C., Dessauges-Zavadsky, M., D’Odorico, S., Kim, T.-S., & McMahon, R. G. 2007, MNRAS, 382, 177
 Péroux, C., Meiring, J. D., Kulkarni, V. P., et al. 2006, MNRAS, 372, 369
 Péroux, C., Meiring, J. D., Kulkarni, V. P., et al. 2008, MNRAS, 386, 2209
 Petitjean, P. & Bergeron, J. 1990, A&A, 231, 309
 Petitjean, P., Srianand, R., & Ledoux, C. 2000, A&A, 364, L26
 Pettini, M., Ellison, S. L., Steidel, C. C., & Bowen, D. V. 1999, ApJ, 510, 576
 Pettini, M., Ellison, S. L., Steidel, C. C., Shapley, A. E., & Bowen, D. V. 2000, ApJ, 532, 65
 Pettini, M., Smith, L. J., Hunstead, R. W., & King, D. L. 1994, ApJ, 426, 79
 Phillips, A. P., Gondhalekar, P. M., & Pettini, M. 1982, MNRAS, 200, 687
 Phillips, A. P., Pettini, M., & Gondhalekar, P. M. 1984, MNRAS, 206, 337
 Planck Collaboration, Ade, P. A. R., Aghanim, N., et al. 2016, A&A, 594, A13

- Pontzen, A., Governato, F., Pettini, M., et al. 2008, MNRAS, 390, 1349
- Pontzen, A. & Pettini, M. 2009, MNRAS, 393, 557
- Primas, F., Brugamyer, E., Sneden, C., et al. 2000, in *The First Stars*, ed. A. Weiss, T. G. Abel, & V. Hill, 51
- Prochaska, J. X., Chen, H., Wolfe, A. M., Dessauges-Zavadsky, M., & Bloom, J. S. 2008, ApJ, 672, 59
- Prochaska, J. X., Gawiser, E., Wolfe, A. M., Castro, S., & Djorgovski, S. G. 2003, ApJ, 595, L9
- Prochaska, J. X., Herbert-Fort, S., & Wolfe, A. M. 2005, ApJ, 635, 123
- Prochaska, J. X. & Wolfe, A. M. 2002, ApJ, 566, 68
- Quiret, S., Péroux, C., Zafar, T., et al. 2016, MNRAS, 458, 4074
- Rafelski, M., Neeleman, M., Fumagalli, M., Wolfe, A. M., & Prochaska, J. X. 2014, ApJ, 782, L29
- Rafelski, M., Wolfe, A. M., Prochaska, J. X., Neeleman, M., & Mendez, A. J. 2012, ApJ, 755, 89
- Rao, S. M., Prochaska, J. X., Howk, J. C., & Wolfe, A. M. 2005, AJ, 129, 9
- Rao, S. M. & Turnshek, D. A. 2000, ApJS, 130, 1
- Rao, S. M., Turnshek, D. A., Sardane, G. M., & Monier, E. M. 2017, MNRAS, 471, 3428
- Rodríguez, E., Petitjean, P., Aracil, B., Ledoux, C., & Srianand, R. 2006, A&A, 446, 791
- Savage, B. D., Cardelli, J. A., & Sofia, U. J. 1992, ApJ, 401, 706
- Savage, B. D. & Sembach, K. R. 1991, ApJ, 379, 245
- Savage, B. D. & Sembach, K. R. 1996, ARA&A, 34, 279
- Savaglio, S. 2001, in *IAU Symposium, Vol. 204, The Extragalactic Infrared Background and its Cosmological Implications*, ed. M. Harwit & M. G. Hauser, 307
- Savaglio, S. 2006, *New Journal of Physics*, 8, 195
- Savaglio, S. 2015, *Journal of High Energy Astrophysics*, 7, 95
- Skúladóttir, Á., Tolstoy, E., Salvadori, S., Hill, V., & Pettini, M. 2017, ArXiv e-prints [arXiv:1708.00511]
- Sneden, C., Gratton, R. G., & Crocker, D. A. 1991, A&A, 246, 354
- Som, D., Kulkarni, V. P., Meiring, J., et al. 2013, MNRAS, 435, 1469
- Thomas, R. C. & Kantowski, R. 2000, Phys. Rev. D, 62, 103507
- Tolstoy, E., Hill, V., & Tosi, M. 2009, ARA&A, 47, 371
- Tremaine, S., Gebhardt, K., Bender, R., et al. 2002, ApJ, 574, 740
- Tremonti, C. A., Heckman, T. M., Kauffmann, G., et al. 2004, ApJ, 613, 898
- Tumlinson, J. 2010, ApJ, 708, 1398
- Tumlinson, J., Peebles, M. S., & Werk, J. K. 2017, ARA&A, 55, 389
- Viegas, S. M. 1995, MNRAS, 276, 268
- Vladilo, G. 1998, ApJ, 493, 583
- Vladilo, G. 2002, A&A, 391, 407
- Vladilo, G., Abate, C., Yin, J., Cescutti, G., & Matteucci, F. 2011, A&A, 530, A33
- Vladilo, G., Centurión, M., Bonifacio, P., & Howk, J. C. 2001, ApJ, 557, 1007
- Vladilo, G. & Péroux, C. 2005, A&A, 444, 461
- Vladilo, G., Prochaska, J. X., & Wolfe, A. M. 2008, A&A, 478, 701
- Vreeswijk, P. M., Ledoux, C., Raassen, A. J. J., et al. 2013, A&A, 549, A22
- Welty, D. E., Hobbs, L. M., Lauroesch, J. T., Morton, D. C., & York, D. G. 1995, ApJ, 449, L135
- Williams, M. J., Bureau, M., & Cappellari, M. 2010, MNRAS, 409, 1330
- Wiseman, P., Schady, P., Bolmer, J., et al. 2017, A&A, 599, A24
- Wolfe, A. M., Gawiser, E., & Prochaska, J. X. 2005, ARA&A, 43, 861
- Wolfe, A. M., Lanzetta, K. M., Foltz, C. B., & Chaffee, F. H. 1995, ApJ, 454, 698

Appendix A: Tables of dust-corrected metallicities

Table A.1. Dust-corrected metallicities and depletions for the clean sample. The original abundances are sourced from Ellison et al. (2012), Péroux et al. (2006), Pettini et al. (2000), Péroux et al. (2008), Rao et al. (2005), Meiring et al. (2011), Pettini et al. (1999), Ledoux et al. (2006), Rafelski et al. (2012), Møller et al. (2013), Ma et al. (2015), and Fynbo et al. (2017). Additional metallicities and depletions are already reported in De Cia et al. (2016).

ID	z	$N(\text{H I})$	$[\text{Fe}/\text{H}]_{\text{tot}}$	$[\text{Zn}/\text{Fe}]_{\text{exp}}$	δ_{Zn}	δ_{Si}	δ_{Fe}	$[\text{X}/\text{Fe}]$	X
B0105-008	1.371	21.70 ± 0.15	-1.35 ± 0.15	0.18	-0.05	-0.15	-0.24	0.18 ± 0.05	Zn
J0256+0110	0.725	20.70 ± 0.20	0.13 ± 0.36	0.90	-0.24	-0.60	-1.15	0.90 ± 0.30	Zn
Q0302-223	1.009	20.36 ± 0.11	-0.36 ± 0.12	0.62	-0.17	-0.42	-0.79	0.62 ± 0.07	Zn
Q0449-1645	1.007	20.98 ± 0.06	-0.88 ± 0.06	0.37	-0.10	-0.26	-0.48	0.37 ± 0.07	Zn
Q0454+039	0.860	20.69 ± 0.06	-0.98 ± 0.08	0.00	-0.00	-0.03	-0.01	0.00 ± 0.11	Zn
Q0933+733	1.479	21.62 ± 0.10	-1.44 ± 0.10	0.37	-0.10	-0.26	-0.47	0.37 ± 0.02	Zn
Q0948+433	1.233	21.62 ± 0.05	-0.97 ± 0.05	0.43	-0.12	-0.30	-0.55	0.43 ± 0.02	Zn
J1009+0713	0.114	20.68 ± 0.10	-0.71 ± 0.20	0.06	-0.02	-0.07	-0.08	0.30 ± 0.21	S
J1107+0048	0.740	21.00 ± 0.04	-0.45 ± 0.04	0.38	-0.10	-0.26	-0.48	0.38 ± 0.15	Zn
Q1354+258	1.420	21.54 ± 0.06	-1.47 ± 0.12	0.41	-0.11	-0.28	-0.52	0.41 ± 0.18	Zn
J1431+3952	0.602	21.20 ± 0.10	-0.59 ± 0.15	0.72	-0.20	-0.48	-0.92	0.72 ± 0.22	Zn
J1623+0718	1.336	21.35 ± 0.10	-0.93 ± 0.11	0.47	-0.13	-0.33	-0.61	0.47 ± 0.10	Zn
J2328+0022	0.652	20.32 ± 0.06	-0.39 ± 0.06	0.43	-0.12	-0.30	-0.55	0.43 ± 0.15	Zn
B2355-106	1.172	21.00 ± 0.10	-0.72 ± 0.14	0.53	-0.14	-0.36	-0.67	0.53 ± 0.20	Zn
J1211+0833	2.117	21.00 ± 0.20	0.42 ± 0.20	1.65	-0.45	-1.06	-2.10	1.65 ± 0.07	Zn
eHAQ0111+0641	2.027	21.50 ± 0.30	-0.47 ± 0.32	0.54	-0.15	-0.37	-0.69	0.54 ± 0.14	Zn
J0817+1351	4.258	21.30 ± 0.15	-1.19 ± 0.16	-0.08	0.00	0.00	0.00	0.19 ± 0.22	S
J1051+3107	4.139	20.70 ± 0.20	-1.98 ± 0.20	0.05	-0.01	-0.06	-0.07	0.29 ± 0.29	S
J1200+4015	3.220	20.85 ± 0.10	-0.56 ± 0.11	0.28	-0.08	-0.21	-0.36	0.47 ± 0.15	S
J1438+4314	4.399	20.89 ± 0.15	-0.97 ± 0.15	0.67	-0.18	-0.45	-0.86	0.77 ± 0.21	S
J1541+3153	2.444	20.95 ± 0.10	-1.06 ± 0.15	0.62	-0.17	-0.42	-0.79	0.57 ± 0.19	Si
J1607+1604	4.474	20.30 ± 0.15	-1.54 ± 0.16	-0.19	0.00	0.00	0.00	0.17 ± 0.22	Si

Table A.2. Dust-corrected metallicities and depletions for the large sample. The original abundances are sourced from Berg et al. (2015) and references therein, Ma et al. (2015), and Fynbo et al. (2017). Additional metallicities and depletions are already reported in De Cia et al. (2016).

ID	z	$N(\text{H I})$	$[\text{Fe}/\text{H}]_{\text{tot}}$	$[\text{Zn}/\text{Fe}]_{\text{exp}}$	δ_{Zn}	δ_{Si}	δ_{Fe}	$[\text{X}/\text{Fe}]$	X
SDSSJ1616+	0.321	20.60 ± 0.20	-0.28 ± 0.21	0.57	-0.15	-0.38	-0.72	0.69 ± 0.12	S
SDSSJ1619+	0.096	20.55 ± 0.10	-0.30 ± 0.18	1.02	-0.28	-0.67	-1.30	1.04 ± 0.17	S
Q1328+307	0.692	21.25 ± 0.10	-1.00 ± 0.14	0.58	-0.16	-0.40	-0.74	0.58 ± 0.00	Zn
Q1137+3907	0.720	21.10 ± 0.10	-0.06 ± 0.11	0.82	-0.22	-0.55	-1.05	0.82 ± 0.00	Zn
J1431+3952	0.602	21.20 ± 0.10	-0.59 ± 0.15	0.72	-0.20	-0.48	-0.92	0.72 ± 0.00	Zn
J2328+0022	0.652	20.32 ± 0.07	-0.39 ± 0.07	0.43	-0.12	-0.30	-0.55	0.43 ± 0.00	Zn
J0256+0110	0.725	20.70 ± 0.16	0.13 ± 0.34	0.90	-0.24	-0.60	-1.15	0.90 ± 0.00	Zn
B0105-008	1.371	21.70 ± 0.15	-1.35 ± 0.15	0.18	-0.05	-0.15	-0.24	0.18 ± 0.00	Zn
J1107+0048	0.740	21.00 ± 0.05	-0.45 ± 0.05	0.37	-0.10	-0.26	-0.48	0.37 ± 0.00	Zn
Q1010+0003	1.265	21.52 ± 0.07	-1.04 ± 0.09	0.54	-0.15	-0.37	-0.69	0.54 ± 0.00	Zn
Q0302-223	1.009	20.36 ± 0.11	-0.36 ± 0.12	0.62	-0.17	-0.42	-0.79	0.62 ± 0.00	Zn
Q1727+5302	1.031	21.41 ± 0.15	-1.06 ± 0.15	0.79	-0.21	-0.53	-1.01	0.79 ± 0.00	Zn
Q1727+5302	0.945	21.16 ± 0.10	-0.31 ± 0.10	0.80	-0.22	-0.53	-1.02	0.80 ± 0.00	Zn
B2355-106	1.173	21.00 ± 0.10	-0.72 ± 0.14	0.52	-0.14	-0.36	-0.67	0.52 ± 0.00	Zn
J1623+0718	1.336	21.35 ± 0.10	-0.93 ± 0.11	0.47	-0.13	-0.33	-0.61	0.47 ± 0.00	Zn
HE0515-441	1.150	20.45 ± 0.15	-0.79 ± 0.25	0.64	-0.17	-0.43	-0.82	0.64 ± 0.00	Zn
J1142+0701	1.841	21.50 ± 0.15	-0.65 ± 0.16	0.66	-0.18	-0.45	-0.85	0.66 ± 0.00	Zn
Q0948+433	1.233	21.62 ± 0.06	-0.97 ± 0.06	0.43	-0.12	-0.30	-0.55	0.43 ± 0.00	Zn
J1056+1208	1.610	21.45 ± 0.15	-0.09 ± 0.16	0.79	-0.21	-0.53	-1.01	0.79 ± 0.00	Zn
Q0151+0448	1.934	20.36 ± 0.10	-1.84 ± 0.10	0.02	-0.01	-0.04	-0.03	0.27 ± 0.05	Si
J1310+5424	1.801	21.45 ± 0.15	-0.29 ± 0.16	0.77	-0.21	-0.51	-0.98	0.77 ± 0.00	Zn
Q0935+417	1.373	20.52 ± 0.10	-0.80 ± 0.14	0.28	-0.08	-0.21	-0.37	0.28 ± 0.00	Zn
J0008-0958	1.768	20.85 ± 0.15	-0.00 ± 0.16	0.53	-0.14	-0.36	-0.68	0.53 ± 0.00	Zn

J1454+0941	1.788	20.50 ± 0.15	-0.24 ± 0.19	0.54	-0.15	-0.37	-0.69	0.54 ± 0.00	Zn
SDSS1435+0	1.656	21.25 ± 0.15	-1.00 ± 0.17	-0.16	0.00	0.00	0.00	0.18 ± 0.10	Si
J0958+0145	1.928	20.40 ± 0.10	-0.85 ± 0.11	0.63	-0.17	-0.42	-0.80	0.57 ± 0.08	Si
Q1157+014	1.944	21.70 ± 0.10	-1.09 ± 0.11	0.46	-0.13	-0.32	-0.59	0.46 ± 0.00	Zn
Q1354+258	1.420	21.54 ± 0.06	-1.46 ± 0.07	0.42	-0.11	-0.30	-0.54	0.42 ± 0.00	Zn
J1417+4132	1.951	21.45 ± 0.25	-0.29 ± 0.25	0.81	-0.22	-0.54	-1.03	0.81 ± 0.00	Zn
J1042+0628	1.943	20.70 ± 0.15	-0.91 ± 0.21	0.21	-0.06	-0.16	-0.26	0.36 ± 0.17	Si
J0233+0103	1.785	20.60 ± 0.15	-1.33 ± 0.16	-0.30	0.00	0.00	0.00	0.11 ± 0.07	Si
J1305+0924	2.018	20.40 ± 0.15	-0.23 ± 0.21	0.49	-0.13	-0.34	-0.62	0.50 ± 0.15	Si
Q1331+17	1.776	21.14 ± 0.08	-1.02 ± 0.09	0.75	-0.20	-0.50	-0.96	0.75 ± 0.00	Zn
Q0013-004	1.973	20.83 ± 0.05	-0.50 ± 0.06	0.77	-0.21	-0.51	-0.98	0.77 ± 0.00	Zn
J2340-00	2.054	20.35 ± 0.15	-0.20 ± 0.16	0.49	-0.13	-0.34	-0.63	0.49 ± 0.00	Zn
Q1755+578	1.971	21.40 ± 0.15	0.08 ± 0.16	0.90	-0.24	-0.60	-1.15	0.90 ± 0.00	Zn
J1509+1113	2.028	21.30 ± 0.15	-0.68 ± 0.17	0.53	-0.14	-0.36	-0.68	0.52 ± 0.09	Si
J1049-0110	1.658	20.35 ± 0.15	0.41 ± 0.16	0.81	-0.22	-0.54	-1.03	0.81 ± 0.00	Zn
SDSS1249-0	1.781	21.45 ± 0.15	-0.78 ± 0.15	0.52	-0.14	-0.36	-0.67	0.52 ± 0.00	Zn
J1024+0600	1.895	20.60 ± 0.15	-0.34 ± 0.17	0.49	-0.13	-0.34	-0.62	0.50 ± 0.09	Si
Q0010-002	2.025	20.95 ± 0.10	-1.24 ± 0.10	-0.15	0.00	0.00	0.00	-0.15 ± 0.00	Zn
Q2230+025	1.864	20.83 ± 0.05	-0.52 ± 0.07	0.45	-0.12	-0.31	-0.58	0.45 ± 0.00	Zn
Q2222-3939	2.154	20.85 ± 0.10	-1.76 ± 0.10	-0.33	0.00	0.00	0.00	-0.00 ± 0.04	S
Q2228-3954	2.095	21.20 ± 0.10	-1.26 ± 0.10	0.18	-0.05	-0.15	-0.24	0.18 ± 0.00	Zn
Q0425-5214	2.224	20.30 ± 0.10	-1.37 ± 0.10	0.26	-0.07	-0.19	-0.33	0.45 ± 0.04	S
Q0450-13	2.067	20.53 ± 0.08	-1.35 ± 0.08	0.18	-0.05	-0.14	-0.24	0.35 ± 0.04	Si
Q0049-2820	2.071	20.45 ± 0.10	-1.31 ± 0.10	-0.20	0.00	0.00	0.00	0.16 ± 0.05	Si
Q0254-4025	2.046	20.45 ± 0.08	-1.59 ± 0.08	0.02	-0.01	-0.04	-0.03	0.27 ± 0.04	S
Q0421-2624	2.157	20.65 ± 0.10	-1.71 ± 0.10	0.16	-0.04	-0.13	-0.21	0.34 ± 0.01	Si
Q0458-0203	2.040	21.65 ± 0.09	-0.98 ± 0.10	0.59	-0.16	-0.40	-0.76	0.59 ± 0.00	Zn
HE1104-180	1.662	20.85 ± 0.01	-0.84 ± 0.02	0.55	-0.15	-0.38	-0.71	0.55 ± 0.00	Zn
Q0551-366	1.962	20.50 ± 0.08	0.13 ± 0.09	0.81	-0.22	-0.54	-1.03	0.81 ± 0.00	Zn
Q0300-3152	2.179	20.80 ± 0.10	-1.79 ± 0.10	0.10	-0.03	-0.09	-0.13	0.33 ± 0.04	S
HE1122-164	0.680	20.45 ± 0.05	-0.24 ± 0.05	1.04	-0.28	-0.68	-1.32	0.77 ± 0.12	Si
J0035-0918	2.340	20.55 ± 0.10	-2.50 ± 0.11	0.00	-0.00	-0.03	-0.01	0.26 ± 0.07	Si
J0035-0918	2.340	20.55 ± 0.10	-2.31 ± 0.12	0.27	-0.07	-0.20	-0.34	0.39 ± 0.08	Si
Q0149+33	2.141	20.50 ± 0.10	-1.59 ± 0.10	0.14	-0.04	-0.12	-0.19	0.14 ± 0.00	Zn
SDSS1042+0	2.267	20.75 ± 0.15	-0.90 ± 0.20	0.18	-0.05	-0.14	-0.24	0.35 ± 0.16	Si
B2314-409	1.857	20.90 ± 0.10	-0.92 ± 0.14	0.28	-0.08	-0.21	-0.37	0.28 ± 0.00	Zn
Q2311-3721	2.182	20.55 ± 0.07	-1.56 ± 0.08	0.04	-0.01	-0.06	-0.06	0.28 ± 0.05	Si
Q0039-3354	2.224	20.60 ± 0.10	-1.21 ± 0.11	0.29	-0.08	-0.21	-0.37	0.40 ± 0.06	Si
Q0027-1836	2.402	21.75 ± 0.10	-1.41 ± 0.10	0.66	-0.18	-0.45	-0.85	0.66 ± 0.00	Zn
Q0201+365	2.463	20.38 ± 0.05	-0.44 ± 0.05	0.30	-0.08	-0.22	-0.39	0.30 ± 0.00	Zn
J0058+0115	2.010	21.10 ± 0.15	-0.60 ± 0.16	0.61	-0.17	-0.41	-0.78	0.61 ± 0.00	Zn
Q0841+12	2.375	20.99 ± 0.08	-1.47 ± 0.08	0.18	-0.05	-0.15	-0.24	0.18 ± 0.00	Zn
Q0841+12	2.476	20.78 ± 0.08	-1.71 ± 0.09	0.03	-0.01	-0.05	-0.05	0.03 ± 0.00	Zn
Q2343+12	2.431	20.34 ± 0.10	-0.60 ± 0.10	0.42	-0.11	-0.30	-0.54	0.42 ± 0.00	Zn
Q0933+733	1.479	21.62 ± 0.10	-1.44 ± 0.10	0.36	-0.10	-0.26	-0.47	0.36 ± 0.00	Zn
J0234-0751	2.318	20.90 ± 0.10	-1.91 ± 0.10	-0.32	0.00	0.00	0.00	0.10 ± 0.09	Si
Q1210+17	1.892	20.63 ± 0.08	-0.78 ± 0.09	0.23	-0.06	-0.18	-0.30	0.23 ± 0.00	Zn
SDSS2059-0	2.210	20.80 ± 0.20	-0.26 ± 0.23	0.78	-0.21	-0.52	-1.00	0.78 ± 0.00	Zn
J1541+3153	2.444	20.95 ± 0.10	-1.45 ± 0.15	0.37	-0.10	-0.26	-0.48	0.37 ± 0.00	Zn
J2321+1421	2.573	20.70 ± 0.05	-1.76 ± 0.06	-0.06	0.00	0.00	0.00	0.23 ± 0.05	Si
Q2206-199	2.076	20.43 ± 0.04	-2.16 ± 0.04	0.04	-0.01	-0.06	-0.06	0.28 ± 0.01	Si
Q2206-199	1.920	20.65 ± 0.07	-0.23 ± 0.07	0.45	-0.12	-0.31	-0.58	0.45 ± 0.00	Zn
J1238+3437	2.471	20.80 ± 0.10	-2.05 ± 0.10	-0.08	0.00	0.00	0.00	0.19 ± 0.11	S
Q1232+082	2.338	20.90 ± 0.10	-0.57 ± 0.13	0.87	-0.24	-0.58	-1.11	0.87 ± 0.00	Zn
J2036-0553	2.280	21.20 ± 0.15	-1.63 ± 0.19	0.12	-0.03	-0.11	-0.16	0.32 ± 0.12	Si
Q1215+33	1.999	20.95 ± 0.07	-1.13 ± 0.09	0.42	-0.11	-0.30	-0.54	0.42 ± 0.00	Zn
SDSSJ1558+	2.553	20.30 ± 0.04	-2.31 ± 0.07	-0.10	0.00	0.00	0.00	0.21 ± 0.06	Si

Q0432-4401	2.302	20.95 ± 0.10	-1.18 ± 0.14	0.23	-0.06	-0.17	-0.29	0.37 ± 0.12	Si
Q0449-1645	1.007	20.98 ± 0.07	-0.88 ± 0.07	0.37	-0.10	-0.26	-0.48	0.37 ± 0.00	Zn
Q0100+13	2.309	21.37 ± 0.08	-1.47 ± 0.08	0.22	-0.06	-0.17	-0.29	0.22 ± 0.00	Zn
Q0836+11	2.465	20.58 ± 0.10	-1.24 ± 0.10	0.02	-0.01	-0.04	-0.03	0.27 ± 0.05	Si
FJ0812+32	2.067	21.00 ± 0.10	-1.37 ± 0.10	0.16	-0.04	-0.13	-0.21	0.16 ± 0.00	Zn
FJ0812+32	2.626	21.35 ± 0.10	-0.58 ± 0.11	0.90	-0.24	-0.60	-1.15	0.90 ± 0.00	Zn
UM673A	1.626	20.70 ± 0.10	-1.59 ± 0.10	-0.32	0.00	0.00	0.00	-0.32 ± 0.00	Zn
Q2344+12	2.538	20.36 ± 0.10	-1.61 ± 0.10	-0.30	0.00	0.00	0.00	0.11 ± 0.03	Si
J1241+4617	2.667	20.70 ± 0.10	-1.88 ± 0.11	-0.59	0.00	0.00	0.00	-0.03 ± 0.04	Si
SDSS1048+3	2.296	20.70 ± 0.10	-2.13 ± 0.22	-0.20	0.00	0.00	0.00	0.16 ± 0.36	Si
Q0528-2505	2.812	21.20 ± 0.04	-0.37 ± 0.04	0.64	-0.17	-0.43	-0.82	0.64 ± 0.00	Zn
Q0528-2505	2.141	20.95 ± 0.05	-1.26 ± 0.10	0.24	-0.07	-0.18	-0.32	0.24 ± 0.00	Zn
Q0913+072	2.618	20.34 ± 0.04	-2.38 ± 0.04	0.02	-0.01	-0.04	-0.03	0.27 ± 0.01	Si
Q2359-02	2.095	20.70 ± 0.10	-0.54 ± 0.10	0.83	-0.23	-0.55	-1.06	0.83 ± 0.00	Zn
Q2359-02	2.154	20.35 ± 0.10	-1.46 ± 0.11	0.27	-0.07	-0.20	-0.34	0.39 ± 0.06	Si
Q0112+030	2.423	20.90 ± 0.10	-1.22 ± 0.10	0.16	-0.04	-0.13	-0.21	0.34 ± 0.06	Si
J1017+6116	2.768	20.60 ± 0.10	-2.01 ± 0.11	-0.24	0.00	0.00	0.00	0.14 ± 0.06	Si
J1558-0031	2.703	20.67 ± 0.05	-1.79 ± 0.06	-0.34	0.00	0.00	0.00	0.09 ± 0.04	Si
Q1409+095	2.456	20.53 ± 0.08	-1.97 ± 0.08	-0.02	0.00	-0.02	0.00	0.25 ± 0.03	Si
J1456+0407	2.674	20.35 ± 0.10	-2.02 ± 0.14	0.39	-0.10	-0.27	-0.50	0.45 ± 0.12	Si
HS1132+224	2.783	21.00 ± 0.07	-1.77 ± 0.07	0.35	-0.09	-0.25	-0.44	0.43 ± 0.12	Si
J1358+0349	2.853	20.50 ± 0.10	-2.52 ± 0.11	-0.02	0.00	-0.02	0.00	0.25 ± 0.18	Si
J1135-0010	2.207	22.05 ± 0.10	-0.86 ± 0.10	0.70	-0.19	-0.47	-0.90	0.70 ± 0.00	Zn
Q0933-3319	2.682	20.50 ± 0.10	-1.30 ± 0.13	0.08	-0.02	-0.08	-0.11	0.30 ± 0.13	Si
J1131+6044	2.875	20.50 ± 0.15	-1.06 ± 0.15	0.88	-0.24	-0.58	-1.11	0.69 ± 0.13	Si
CTQ418	2.514	20.50 ± 0.07	-1.38 ± 0.08	0.31	-0.08	-0.22	-0.39	0.41 ± 0.04	Si
Q0201+36	2.463	20.38 ± 0.04	-0.07 ± 0.06	0.59	-0.16	-0.40	-0.76	0.59 ± 0.00	Zn
CTQ418	2.429	20.68 ± 0.07	-1.72 ± 0.09	0.23	-0.06	-0.17	-0.29	0.37 ± 0.06	Si
J1340+1106	2.796	21.00 ± 0.06	-1.75 ± 0.06	0.12	-0.03	-0.11	-0.16	0.32 ± 0.02	Si
Q1337+113	2.796	21.00 ± 0.08	-1.73 ± 0.08	0.14	-0.04	-0.12	-0.19	0.33 ± 0.04	Si
SDSS2222-0	2.354	20.50 ± 0.15	-0.26 ± 0.17	0.65	-0.18	-0.44	-0.83	0.58 ± 0.09	Si
Q2348-1444	2.279	20.59 ± 0.08	-1.85 ± 0.09	0.08	-0.02	-0.08	-0.11	0.30 ± 0.08	Si
Q1223+1753	2.466	21.50 ± 0.10	-1.52 ± 0.10	0.23	-0.06	-0.18	-0.30	0.23 ± 0.00	Zn
J0211+1241	2.595	20.60 ± 0.15	-0.64 ± 0.16	0.35	-0.09	-0.25	-0.44	0.43 ± 0.09	Si
Q2318-1107	1.989	20.68 ± 0.05	-0.68 ± 0.05	0.43	-0.12	-0.30	-0.55	0.43 ± 0.00	Zn
SDSS0225+0	2.714	21.00 ± 0.15	-0.61 ± 0.17	0.43	-0.12	-0.30	-0.55	0.43 ± 0.00	Zn
J1304+1202	2.929	20.30 ± 0.15	-1.55 ± 0.15	0.19	-0.05	-0.15	-0.25	0.40 ± 0.05	S
J1304+1202	2.913	20.55 ± 0.15	-1.49 ± 0.16	0.54	-0.15	-0.37	-0.69	0.67 ± 0.06	S
SDSS1116+4	2.662	20.48 ± 0.10	-0.46 ± 0.14	0.88	-0.24	-0.58	-1.12	0.88 ± 0.00	Zn
Q0112-306	2.418	20.50 ± 0.08	-2.19 ± 0.09	-0.16	0.00	0.00	0.00	0.18 ± 0.04	Si
Q0112-306	2.702	20.30 ± 0.10	-0.41 ± 0.12	0.55	-0.15	-0.37	-0.70	0.53 ± 0.08	Si
Q0216+0803	2.293	20.40 ± 0.08	-0.48 ± 0.09	0.40	-0.11	-0.28	-0.52	0.40 ± 0.00	Zn
J1356-1101	2.967	20.80 ± 0.10	-1.44 ± 0.11	0.04	-0.01	-0.06	-0.06	0.28 ± 0.09	Si
Q1354-1046	2.501	20.44 ± 0.05	-1.44 ± 0.09	-0.17	0.00	0.00	0.00	0.12 ± 0.12	S
J1712+5755	2.253	20.60 ± 0.10	-1.17 ± 0.10	0.27	-0.07	-0.20	-0.34	0.39 ± 0.06	Si
Q1354-1046	2.967	20.80 ± 0.10	-1.40 ± 0.11	0.08	-0.02	-0.08	-0.11	0.30 ± 0.04	Si
Q2348-01	2.426	20.50 ± 0.10	-0.33 ± 0.10	0.94	-0.25	-0.62	-1.19	0.72 ± 0.02	Si
Q2348-01	2.615	21.30 ± 0.10	-1.87 ± 0.13	0.04	-0.01	-0.06	-0.06	0.28 ± 0.11	Si
Q2342+34	2.908	21.10 ± 0.10	-0.67 ± 0.12	0.84	-0.23	-0.55	-1.06	0.67 ± 0.09	Si
HE2243-603	2.330	20.67 ± 0.02	-1.03 ± 0.02	0.14	-0.04	-0.12	-0.19	0.14 ± 0.00	Zn
Q0405-443	2.550	21.13 ± 0.10	-1.22 ± 0.12	0.33	-0.09	-0.24	-0.43	0.33 ± 0.00	Zn
Q2231-00	2.066	20.53 ± 0.08	-0.76 ± 0.09	0.31	-0.09	-0.23	-0.40	0.31 ± 0.00	Zn
Q0405-443	2.595	21.09 ± 0.10	-0.93 ± 0.10	0.37	-0.10	-0.26	-0.48	0.37 ± 0.00	Zn
Q0405-443	2.622	20.47 ± 0.10	-1.84 ± 0.10	0.18	-0.05	-0.14	-0.24	0.35 ± 0.06	Si
J1419+0829	3.050	20.40 ± 0.03	-2.02 ± 0.04	-0.02	0.00	-0.02	0.00	0.25 ± 0.03	Si
Q0102-190	2.370	21.00 ± 0.08	-1.88 ± 0.08	-0.07	0.00	0.00	0.00	0.20 ± 0.03	S
J1004+0018	2.685	21.39 ± 0.10	-1.87 ± 0.11	0.10	-0.03	-0.09	-0.13	0.33 ± 0.04	S

J1004+0018	2.540	21.30 ± 0.10	-1.44 ± 0.10	0.06	-0.02	-0.07	-0.08	0.30 ± 0.02	S
Q1759+75	2.625	20.76 ± 0.05	-0.79 ± 0.05	0.31	-0.08	-0.22	-0.39	0.41 ± 0.03	Si
SDSS1043+6	2.786	20.60 ± 0.15	-1.82 ± 0.25	-0.40	0.00	0.00	0.00	0.06 ± 0.36	Si
J1037+0139	2.705	20.50 ± 0.08	-1.82 ± 0.08	0.29	-0.08	-0.21	-0.37	0.40 ± 0.04	Si
SDSS1003+5	2.502	20.35 ± 0.15	-1.27 ± 0.34	1.22	-0.33	-0.79	-1.55	0.86 ± 0.42	Si
Q0918+1636	2.412	21.26 ± 0.06	-0.49 ± 0.24	0.56	-0.15	-0.38	-0.72	0.56 ± 0.00	Zn
Q0918+1636	2.583	20.96 ± 0.05	0.05 ± 0.05	0.81	-0.22	-0.54	-1.03	0.81 ± 0.00	Zn
Q0058-292	2.671	21.10 ± 0.10	-1.40 ± 0.10	0.33	-0.09	-0.24	-0.43	0.33 ± 0.00	Zn
Q2059-360	3.083	20.98 ± 0.08	-1.71 ± 0.11	-0.04	0.00	-0.01	0.00	0.24 ± 0.09	Si
Q0642-5038	2.659	20.95 ± 0.08	-1.83 ± 0.09	0.31	-0.09	-0.23	-0.40	0.31 ± 0.00	Zn
B1036-2257	2.778	20.93 ± 0.05	-1.28 ± 0.05	0.26	-0.07	-0.19	-0.33	0.45 ± 0.02	S
J1240+1455	3.108	21.30 ± 0.20	-0.71 ± 0.20	1.14	-0.31	-0.75	-1.45	1.14 ± 0.00	Zn
J1507+4406	3.064	20.75 ± 0.10	-1.99 ± 0.10	0.03	-0.01	-0.05	-0.05	0.28 ± 0.10	S
Q1021+30	2.949	20.70 ± 0.10	-1.87 ± 0.10	-0.04	0.00	-0.01	0.00	0.24 ± 0.02	Si
Q1036-2257	2.778	20.93 ± 0.05	-1.36 ± 0.05	0.13	-0.03	-0.11	-0.16	0.35 ± 0.01	S
SDSS2100-0	3.092	21.05 ± 0.15	-0.23 ± 0.16	0.71	-0.19	-0.48	-0.91	0.71 ± 0.00	Zn
J1219+1603	3.003	20.35 ± 0.10	-1.78 ± 0.14	-0.45	0.00	0.00	0.00	0.04 ± 0.18	Si
PKS1354-17	2.780	20.30 ± 0.15	-1.45 ± 0.17	0.63	-0.17	-0.42	-0.80	0.57 ± 0.10	Si
J1604+3951	3.163	21.75 ± 0.20	-1.12 ± 0.21	0.49	-0.13	-0.34	-0.63	0.49 ± 0.00	Zn
SDSS0759+3	3.035	20.60 ± 0.10	-1.97 ± 0.22	0.00	-0.00	-0.03	-0.01	0.26 ± 0.36	Si
Q1425+6039	2.827	20.30 ± 0.04	-0.59 ± 0.04	0.54	-0.15	-0.37	-0.69	0.54 ± 0.00	Zn
Q2138-444	2.852	20.98 ± 0.05	-1.67 ± 0.05	0.12	-0.03	-0.11	-0.16	0.12 ± 0.00	Zn
SDSS1251+4	2.730	21.10 ± 0.10	-2.05 ± 0.32	-1.22	0.00	0.00	0.00	-0.34 ± 0.42	Si
Q0336-01	3.062	21.20 ± 0.10	-1.36 ± 0.10	0.23	-0.06	-0.17	-0.30	0.43 ± 0.03	S
SDSS0844+5	2.775	21.45 ± 0.15	-0.70 ± 0.16	0.77	-0.21	-0.51	-0.98	0.64 ± 0.06	Si
Q1502+4837	2.570	20.30 ± 0.15	-1.47 ± 0.19	-0.43	0.00	0.00	0.00	0.05 ± 0.15	Si
Q0135-273	2.800	21.00 ± 0.10	-1.52 ± 0.10	0.00	-0.00	-0.03	-0.01	0.26 ± 0.16	Si
SDSS1610+4	2.508	21.15 ± 0.15	0.01 ± 0.16	0.78	-0.21	-0.52	-1.00	0.78 ± 0.00	Zn
HS0741+474	3.017	20.48 ± 0.10	-1.68 ± 0.10	0.00	-0.00	-0.03	-0.01	0.26 ± 0.01	Si
Q0347-38	3.025	20.63 ± 0.01	-1.41 ± 0.01	0.20	-0.06	-0.16	-0.26	0.20 ± 0.00	Zn
Q1451+123	2.469	20.39 ± 0.10	-1.47 ± 0.12	0.69	-0.19	-0.46	-0.88	0.60 ± 0.14	Si
Q1451+123	2.255	20.30 ± 0.15	-0.97 ± 0.17	0.36	-0.10	-0.26	-0.47	0.36 ± 0.00	Zn
Q0242-2917	2.560	20.90 ± 0.10	-1.86 ± 0.10	-0.21	0.00	0.00	0.00	0.09 ± 0.04	S
J0900+42	3.246	20.30 ± 0.10	-0.82 ± 0.10	0.26	-0.07	-0.19	-0.33	0.45 ± 0.01	S
J1555+4800	2.391	21.50 ± 0.15	-0.25 ± 0.16	0.84	-0.23	-0.55	-1.06	0.67 ± 0.07	Si
Q1209+093	2.584	21.40 ± 0.10	-0.81 ± 0.10	0.54	-0.15	-0.37	-0.69	0.54 ± 0.00	Zn
SDSS1709+3	2.530	20.45 ± 0.15	-1.47 ± 0.25	-0.20	0.00	0.00	0.00	0.16 ± 0.28	Si
FJ2334-090	3.057	20.48 ± 0.05	-0.81 ± 0.06	0.58	-0.16	-0.40	-0.74	0.58 ± 0.00	Zn
J1200+4015	3.220	20.65 ± 0.15	-0.30 ± 0.16	0.39	-0.11	-0.28	-0.50	0.39 ± 0.00	Zn
Q1111-152	3.266	21.30 ± 0.05	-1.51 ± 0.05	0.35	-0.10	-0.25	-0.45	0.35 ± 0.00	Zn
J0142+0023	3.348	20.38 ± 0.05	-1.57 ± 0.11	0.31	-0.08	-0.22	-0.39	0.41 ± 0.10	Si
SDSS1440+0	2.518	21.00 ± 0.15	-1.74 ± 0.34	-1.22	0.00	0.00	0.00	-0.34 ± 0.42	Si
Q0930+28	3.235	20.35 ± 0.10	-2.02 ± 0.10	0.00	-0.00	-0.03	-0.01	0.26 ± 0.04	Si
Q0335-1213	3.180	20.78 ± 0.10	-2.19 ± 0.16	-0.47	0.00	0.00	0.00	0.03 ± 0.16	Si
J1155+0530	3.326	21.05 ± 0.10	-0.68 ± 0.11	0.36	-0.10	-0.26	-0.47	0.36 ± 0.00	Zn
J0825+5127	3.318	20.85 ± 0.10	-1.49 ± 0.10	0.35	-0.09	-0.25	-0.44	0.43 ± 0.10	Si
Q2223+20	3.119	20.30 ± 0.10	-2.07 ± 0.12	0.04	-0.01	-0.06	-0.06	0.28 ± 0.07	Si
Q0201+1120	3.386	21.26 ± 0.10	-1.27 ± 0.14	-0.07	0.00	0.00	0.00	0.20 ± 0.14	S
J1637+2901	3.496	20.70 ± 0.10	-2.02 ± 0.14	-1.48	0.00	0.00	0.00	-0.47 ± 0.17	Si
Q1418-0630	3.448	20.40 ± 0.10	-1.21 ± 0.10	0.31	-0.08	-0.22	-0.39	0.41 ± 0.09	Si
J0909+3303	3.658	20.55 ± 0.10	-1.11 ± 0.10	0.33	-0.09	-0.23	-0.42	0.42 ± 0.09	Si
BR1108-074	3.608	20.37 ± 0.07	-1.57 ± 0.07	0.16	-0.04	-0.13	-0.21	0.34 ± 0.01	Si
BR1117-132	3.350	20.84 ± 0.12	-1.13 ± 0.12	0.27	-0.07	-0.20	-0.35	0.27 ± 0.00	Zn
J0255+00	3.915	21.30 ± 0.05	-1.78 ± 0.10	0.07	-0.02	-0.08	-0.10	0.31 ± 0.09	S
J0255+00	3.253	20.70 ± 0.10	-0.77 ± 0.10	0.53	-0.14	-0.36	-0.68	0.52 ± 0.04	Si
PSS1253-02	2.783	21.85 ± 0.20	-1.64 ± 0.20	0.25	-0.07	-0.19	-0.33	0.25 ± 0.00	Zn
Q0000-262	3.390	21.41 ± 0.08	-2.03 ± 0.09	-0.02	0.00	-0.02	0.00	-0.02 ± 0.00	Zn

J1257-0111	4.021	20.30 ± 0.10	-1.25 ± 0.12	0.61	-0.17	-0.41	-0.78	0.56 ± 0.07	Si
J1111+3509	4.052	20.80 ± 0.15	-1.87 ± 0.16	-0.14	0.00	0.00	0.00	0.19 ± 0.07	Si
Q1055+46	3.317	20.34 ± 0.10	-1.64 ± 0.12	0.02	-0.01	-0.04	-0.03	0.27 ± 0.13	Si
SDSS1557+2	3.538	20.65 ± 0.10	-1.64 ± 0.32	0.61	-0.17	-0.41	-0.78	0.56 ± 0.42	Si
PSS1802+56	3.811	20.35 ± 0.20	-1.88 ± 0.22	-0.20	0.00	0.00	0.00	0.16 ± 0.14	Si
PSS1506+52	3.224	20.67 ± 0.07	-2.10 ± 0.08	-0.26	0.00	0.00	0.00	0.13 ± 0.04	Si
PSS2323+27	3.684	20.95 ± 0.10	-2.02 ± 0.16	0.61	-0.17	-0.41	-0.78	0.56 ± 0.13	Si
PSSJ2344+0	3.220	21.25 ± 0.08	-1.65 ± 0.17	0.01	-0.00	-0.04	-0.02	0.01 ± 0.00	Zn
PSSJ0957+3	3.279	20.45 ± 0.08	-0.98 ± 0.08	0.43	-0.12	-0.30	-0.55	0.47 ± 0.05	Si
PSSJ0957+3	4.178	20.70 ± 0.10	-1.53 ± 0.11	0.27	-0.07	-0.20	-0.34	0.39 ± 0.05	Si
J1051+3107	4.139	20.70 ± 0.20	-1.94 ± 0.20	-0.08	0.00	0.00	0.00	0.22 ± 0.04	Si
PSSJ2155+1	3.316	20.50 ± 0.15	-0.97 ± 0.20	0.38	-0.10	-0.27	-0.49	0.38 ± 0.00	Zn
PSSJ1248+3	3.696	20.63 ± 0.07	-1.52 ± 0.09	0.41	-0.11	-0.28	-0.52	0.46 ± 0.05	Si
J0953-0504	4.203	20.55 ± 0.10	-2.51 ± 0.21	-0.04	0.00	-0.01	0.00	0.24 ± 0.19	Si
BR0951-04	3.857	20.60 ± 0.10	-1.18 ± 0.12	0.59	-0.16	-0.40	-0.75	0.55 ± 0.07	Si
J0817+1351	4.258	21.30 ± 0.15	-1.22 ± 0.16	-0.08	0.00	0.00	0.00	0.19 ± 0.06	S
BRI1013+00	3.104	21.10 ± 0.10	-0.11 ± 0.11	0.99	-0.27	-0.65	-1.26	0.99 ± 0.00	Zn
PSS1443+27	4.224	20.95 ± 0.10	-0.57 ± 0.10	0.36	-0.10	-0.25	-0.46	0.53 ± 0.03	S
PSSJ0808+5	3.114	20.65 ± 0.07	-1.46 ± 0.08	0.27	-0.07	-0.20	-0.34	0.39 ± 0.13	Si
PC0953+474	4.243	20.90 ± 0.15	-2.06 ± 0.17	0.06	-0.02	-0.07	-0.09	0.29 ± 0.08	Si
J0834+2140	4.390	21.00 ± 0.20	-1.30 ± 0.20	0.23	-0.06	-0.17	-0.30	0.43 ± 0.04	S
J0834+2140	4.461	20.30 ± 0.15	-1.81 ± 0.17	-0.12	0.00	0.00	0.00	0.20 ± 0.08	Si
Q2237-0608	4.080	20.52 ± 0.11	-1.78 ± 0.16	0.06	-0.02	-0.07	-0.09	0.29 ± 0.12	Si
J1201+2117	3.797	21.35 ± 0.15	-0.68 ± 0.16	0.51	-0.14	-0.35	-0.65	0.51 ± 0.04	Si
J1201+2117	4.158	20.60 ± 0.15	-2.01 ± 0.15	-0.67	0.00	0.00	0.00	-0.07 ± 0.04	Si
J1438+4314	4.399	20.89 ± 0.15	-1.18 ± 0.15	0.52	-0.14	-0.35	-0.66	0.65 ± 0.01	S
J1042+3107	4.087	20.75 ± 0.10	-1.76 ± 0.10	-0.43	0.00	0.00	0.00	0.05 ± 0.03	Si
BR1202-072	4.383	20.55 ± 0.03	-1.44 ± 0.11	0.43	-0.12	-0.30	-0.55	0.47 ± 0.12	Si
J0307-4945	4.466	20.67 ± 0.09	-1.36 ± 0.19	0.35	-0.09	-0.25	-0.44	0.43 ± 0.18	Si
J1607+1604	4.474	20.30 ± 0.15	-1.56 ± 0.16	-0.47	0.00	0.00	0.00	0.03 ± 0.06	Si
J0831+4046	4.344	20.75 ± 0.15	-2.10 ± 0.17	-0.38	0.00	0.00	0.00	0.07 ± 0.08	Si
J1051+3545	4.350	20.45 ± 0.10	-1.72 ± 0.11	0.25	-0.07	-0.18	-0.32	0.38 ± 0.05	Si
J1101+0531	4.345	21.30 ± 0.10	-0.93 ± 0.17	0.51	-0.14	-0.35	-0.65	0.51 ± 0.15	Si
J0824+1302	4.472	20.65 ± 0.20	-2.17 ± 0.22	-0.12	0.00	0.00	0.00	0.20 ± 0.11	Si
J1221+4445	4.811	20.65 ± 0.20	-1.58 ± 0.21	-1.42	0.00	0.00	0.00	-0.44 ± 0.06	Si
J1208+0010	5.082	20.30 ± 0.15	-1.79 ± 0.17	0.37	-0.10	-0.26	-0.47	0.44 ± 0.09	Si
J1211+0833	2.117	21.00 ± 0.20	0.42 ± 0.20	1.65	-0.45	-1.06	-2.10	1.65 ± 0.00	Zn
eHAQ0111+0	2.027	21.50 ± 0.30	-0.47 ± 0.32	0.54	-0.15	-0.37	-0.69	0.54 ± 0.00	Zn